

The seismic structure of the Antarctic upper mantle



Douglas A. Wiens^{1*}, Weisen Shen² and Andrew J. Lloyd³

¹Department of Earth and Planetary Sciences, Washington University in St Louis, St Louis, MO 63130, USA

²Department of Geosciences, Stony Brook University, Stony Brook, NY 11794-2100, USA

³Lamont-Doherty Earth Observatory, Columbia University, Palisades, NY 10964, USA

DAW, 0000-0002-5169-4386; WS, 0000-0002-3766-632X; AJL, 0000-0002-2253-1342

*Correspondence: doug@wustl.edu

Abstract: The deployment of seismic stations and the development of ambient noise tomography as well as new analysis methods provide an opportunity for higher-resolution imaging of Antarctica. Here we review recent seismic structure models and describe their implications for the dynamics and history of the Antarctic upper mantle. Results show that most of East Antarctica is underlain by continental lithosphere to depths of approximately 200 km. The thickest lithosphere is found in a band 500–1000 km inboard from the Transantarctic Mountains, representing the continuation of cratonic lithosphere with Australian affinity beneath the ice. Dronning Maud Land and the Lambert Graben show much thinner lithosphere, consistent with Phanerozoic lithospheric disruption. The Transantarctic Mountains mark a sharp boundary between cratonic lithosphere and the warmer upper mantle of West Antarctica. In the southern Transantarctic Mountains, cratonic lithosphere has been replaced by warm asthenosphere, giving rise to Cenozoic volcanism and an elevated mountainous region. The Marie Byrd Land volcanic dome is underlain by slow seismic velocities extending through the transition zone, consistent with a mantle plume. Slow-velocity anomalies beneath the coast from the Amundsen Sea Embayment to the Antarctic Peninsula are likely to result from upwelling of warm asthenosphere during subduction of the Antarctic–Phoenix spreading centre.

Seismological imaging provides essential constraints on the physical processes and conditions shaping the upper mantle beneath Antarctica. Unlike other continents, the Antarctic mantle is overlain not only by the crust and sedimentary cover, but also by a thick ice sheet, which greatly limits geological mapping and sampling. Thus, seismological studies applied to Antarctica fulfill a unique role by providing information on poorly constrained geological processes that have formed the continent. The ice sheets also constitute large, temporally varying loads that cause deformation of the mantle and the land surface through glacial isostatic adjustment. Seismology is able to characterize lateral variations in the temperature profile of the upper mantle and crust, and thus constrain the geothermal heat flux (Shapiro and Ritzwoller 2004; Shen *et al.* 2020). These thermal properties control the response of the mantle and the land surface to glaciation (Ivins and Sammis 1995; Ivins and James 2005; van der Wal *et al.* 2015; Ivins *et al.* In press), and affect the future evolution of the ice sheet (Gomez *et al.* 2015; Whitehouse *et al.* 2019).

Seismographs were part of the scientific agenda for Antarctic exploration from the very first expeditions. A Milne seismograph was operated by Robert F. Scott's Discovery Expedition (1901–04) for more than a year at Hut Point, near modern-day McMurdo Station, and dozens of earthquakes were detected (Bernacchi and Milne 1908). A seismograph was installed at the South Pole base during the International Geophysical Year in 1957. However, despite these early efforts, it was not until the turn of the century that autonomous seismographs were installed in Antarctica, allowing the underlying structure of the continent to be revealed at greater resolution.

The last two decades have seen rapid progress both in seismological instrumentation in Antarctica and in seismic analysis methods to utilize these data. The results of these efforts are detailed seismological models describing the 3D structure of the Antarctic upper mantle, as well as crustal thickness. Here we review these models and briefly describe their implications for understanding the dynamics and history of the Antarctic upper mantle. This review concentrates on large-scale studies of the upper-mantle structure from analysis of passive seismic recording, while recognizing that active

source seismic studies provide important details in some specific regions.

Seismic data and analysis methods

Antarctic seismic data

From the 1950s through to the 1990s, seismographs were largely restricted to a few permanently occupied bases. With the exception of South Pole, these were generally along the coasts, so the interior of Antarctica was relatively unexplored from a seismological standpoint. Thus, maps of Antarctic mantle structure from that time period showed very limited resolution compared to other parts of the world. Active source seismic refraction lines did provide estimates of crustal thickness and uppermost mantle P-wave velocity in several places (Bentley 1973; ten Brink *et al.* 1993; Leitchenkov and Kudryavtzev 1997; Trey *et al.* 1999).

The advent of technology for operating autonomous broadband seismographs in remote parts of the Antarctic interior has revolutionized seismic studies in Antarctica over the past two decades. Initial projects, including SEPA (Robertson Maurice *et al.* 2003), ANUBIS (Anandakrishnan *et al.* 2000), TAMSEIS (Lawrence *et al.* 2006a), SSCUA (Reading 2006) and a deployment in the Transantarctic Mountains (Bannister *et al.* 2003), generally operated stations only in the summer months. However, more recent large-scale deployments such as AGAP/GAMSEIS (Hansen *et al.* 2010), Ross Ice Shelf (Baker *et al.* 2019), TAMNNET (Hansen *et al.* 2015) and UKANET (O'Donnell *et al.* 2019b) have provided high-quality data throughout the year. In many cases the seismographs remained deployed for only about 2 years, although the POLENET/A-NET project (Accardo *et al.* 2014) has maintained some remote autonomous stations for over a decade. Figure 1 shows the distribution of Antarctic broadband seismic stations providing data for analyses discussed here. The combined distribution of seismic stations provides reasonably good coverage at the several hundred-kilometre level in West Antarctica; however, vast regions of East Antarctica remain without instrumentation.

From: Martin, A. P. and van der Wal, W. (eds) *The Geochemistry and Geophysics of the Antarctic Mantle*.

Geological Society, London, Memoirs, **56**, <https://doi.org/10.1144/M56-2020-18>

© 2021 The Author(s). This is an Open Access article distributed under the terms of the Creative Commons Attribution License (<http://creativecommons.org/licenses/by/4.0/>). Published by The Geological Society of London.

Publishing disclaimer: www.geolsoc.org.uk/pub_ethics

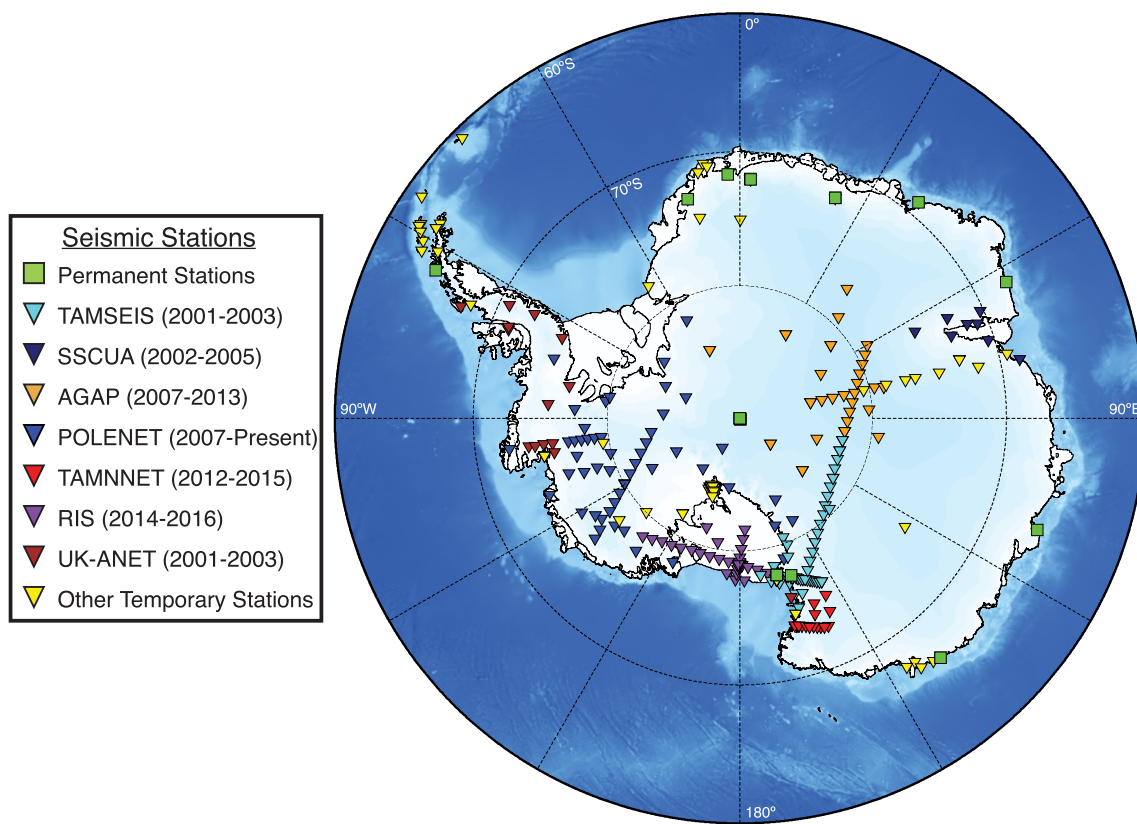


Fig. 1. Map of broadband seismic stations deployed in Antarctica and used in recent seismic studies. Permanent seismic stations, generally at Antarctic research stations, are shown as green boxes, and temporary seismic stations are shown as triangles. The key identifies some of the larger temporary seismic station deployments.

Body-wave tomography and receiver functions

P- and S-wave tomography using teleseismic arrivals can provide strong constraints on lateral velocity variations in the upper mantle of Antarctica (Watson *et al.* 2006; Lloyd *et al.* 2013, 2015; Hansen *et al.* 2014; Brenn *et al.* 2017; White-Gaynor *et al.* 2019; Lucas *et al.* 2020b). In these studies, arrival time anomalies across a seismic array are calculated from P- or S-waveforms using cross-correlation, and the travel time anomalies are then inverted for the velocity structure beneath the array. These studies typically yield detailed images of lateral velocity variations, but provide limited constraints on the depths of the velocity anomalies. Continent-wide body-wave tomography models suffer from highly variable resolution, with good resolution in areas with greater seismic station density, such as parts of West Antarctica, and poor resolution in regions of sparse station coverage.

Body-wave arrivals can also be analysed for structural interfaces or discontinuities below the seismic station using receiver function methodology. This method processes the horizontal and vertical components of body waves to enhance arrivals converted from S to P or P to S at structural interfaces (e.g. Ammon 1991). In general, P-wave receiver functions yield good resolution of Moho depth as well as shallow interfaces, and have provided estimates of crustal thickness for many locations around the continent (Bannister *et al.* 2003; Reading 2006; Chaput *et al.* 2014; Ramirez *et al.* 2017). For some areas with a thick ice sheet, S-wave receiver functions provide better results because the Moho conversion is not obscured by reverberations of seismic energy in the ice (Hansen *et al.* 2009, 2010; Ramirez *et al.* 2016). P-wave receiver functions are also used to study the depth of the 410 and 660 km discontinuities in the mantle, and thus infer the thickness of the transition zone (Reusch *et al.* 2008; Emry *et al.*

2015, 2020). The thickness of the transition zone allows identification of temperature anomalies at transition zone depths due to the different signs of the Clapton slopes of the olivine to wadsleyite and ringwoodite to bridgemanite phase transitions denoted by these discontinuities (e.g. Bina and Helffrich 1994).

Surface waves from earthquakes and ambient noise

Surface-wave tomography can image the crust and upper mantle with superior depth resolution due to the relationship between surface-wave dispersion and velocity structure with depth. However, good resolution is generally limited to the upper 200–250 km of the Earth, and the resulting structures are usually quite smooth, without sharp interfaces. Traditional surface-wave methods involve analysing individual seismograms to determine the surface-wave group and phase velocity along the path from earthquake to receiver, and then performing a tomographic inversion at each period to generate phase and group velocity maps (Roult *et al.* 1994; Danesi and Morelli 2001; Ritzwoller *et al.* 2001). These maps can then be inverted to determine shear velocity at each location. The inclusion of higher-mode Rayleigh-wave measurements improves the resolution at depths of >200 km (Sieminski *et al.* 2003). In some cases, the surface-wave group velocity measurements may be inverted directly for shear velocity (An *et al.* 2015).

Denser arrays of seismographs on the Antarctic interior can be used to determine the phase velocity of Rayleigh waves from teleseismic earthquakes travelling across the continent (Lawrence *et al.* 2006b). In one implementation, the incoming Rayleigh waves are approximated as two interfering plane waves, with seismograms then analysed to determine phase

Seismic structure of the Antarctic upper mantle

velocity images as a function of period, which are then inverted for velocity structure (Forsyth and Li 2005; Heeszel *et al.* 2013, 2016). Surface-wave phase and group velocities can also be measured from seismic Green's functions derived by cross-correlating ambient noise at station pairs. This approach produces more accurate results than measurements from earthquake records at short periods (Shapiro *et al.* 2005; Pyle *et al.* 2010). Phase velocities determined by ambient noise at shorter periods (*c.* 8–45 s) are often combined with phase velocities from earthquakes at longer periods (*c.* 25–120 s) to provide phase velocities across a wide period band, and to constrain both shallow crustal and deeper mantle structure (Shen *et al.* 2018a; O'Donnell *et al.* 2019b). In areas with thinner crust, such as the Ross Embayment, the addition of ambient noise provides key constraints to the uppermost mantle structure.

Seismic anisotropy analysis

Seismic anisotropy, or the directional dependence of seismic velocities resulting from directional dependence of the elastic moduli, has the potential to reveal further information about mantle structure and processes. Seismic anisotropy is often a result of lattice-preferred orientation, which is the alignment of the crystallographic axes of anisotropic minerals by rock fabric or deformation. Alternatively, seismic anisotropy can result from shape-preferred orientation, or the alignment of geometrical objects of different seismic velocity, such as elongated minerals or larger objects such as dykes or sills. Studies of naturally deformed mantle xenoliths (Mainprice and Silver 1993; Chatzaras and Kruckenberg 2021), as well as laboratory studies of artificially deformed olivine aggregates (Zhang and Karato 1995), indicate that mantle seismic anisotropy generally results from lattice-preferred orientation. The fast axis of anisotropy is usually parallel to the extension direction or to the flow direction if there is a flow fabric, although other orientations are possible under conditions of high water or high stress (Karato *et al.* 2008). Thus, mantle anisotropy is commonly used to indicate the extension direction of mantle deformation or the direction of mantle flow.

Seismic observations cannot fully determine the general elastic tensor for anisotropic media, so several different techniques are used to constrain different aspects of anisotropy. Radial anisotropy (transverse isotropy) can be thought of as the difference between vertical (V_{SV}) and horizontally (V_{SH}) polarized shear-wave velocities, and is usually measured by jointly analysing Love and Rayleigh surface waves. The uppermost mantle shows positive radial anisotropy ($V_{SH} > V_{SV}$) in most places worldwide (Panning and Romanowicz 2006; Kustowski *et al.* 2008). Seismic models for Antarctica also show strong positive radial anisotropy (Ritzwoller *et al.* 2001; Lloyd 2018; Zhou *et al.* 2019; O'Donnell *et al.* 2019a), although the spatial pattern is not well resolved.

Azimuthal anisotropy can be evaluated by measuring the variation of P-, S- or surface-wave velocities with azimuth, or by shear-wave splitting measurements. Shear waves propagating through an anisotropic media are split along fast and slow vibration planes, allowing the fast direction and magnitude of anisotropy to be estimated. SKS and SKKS phases from distant earthquakes are particularly useful, since they eliminate the possibility that the anisotropy is near the source, and results are commonly interpreted as upper-mantle anisotropy beneath the receiver (Silver 1996; Savage 1999). Several SKS splitting studies have been carried out in Antarctica (Muller 2001; Bayer *et al.* 2007; Reading and Heintz 2008; Barklage *et al.* 2009; Accardo *et al.* 2014). Results show strong azimuthal anisotropy in parts of West Antarctica (Fig. 2), and indicate that the average upper-mantle azimuthal

anisotropy of West Antarctica is greater than that of East Antarctica (Accardo *et al.* 2014; Lucas *et al.* 2020a). The anisotropy fast directions show a complex pattern related to the tectonic development of the region. The directions do not generally align with the velocity of the Antarctic Plate in an absolute reference frame, indicating that the anisotropy is not due to mantle shear from the continent moving relative to the deeper mantle (Accardo *et al.* 2014).

Bayesian joint inversion

The large-scale collection of broadband seismic data at regional or continental scales over the past two decades has enabled the joint analysis of multiple types of seismic observations. Local surface-wave dispersion properties and P-wave Moho conversion waveforms (i.e. receiver functions) are typical choices since they can be incorporated into a relatively simple local inversion for a 1D model (Julià *et al.* 2000; Chang *et al.* 2004; Lawrence and Wiens 2004). Among various realizations, the joint inversion under the Bayesian framework has been popular, since the associated uncertainties of the resulting 3D model can be quantified from Monte Carlo sampling.

For Antarctica, this approach has been applied to data collected by more than 200 seismic stations deployed between 1998 and 2017. Shen *et al.* (2018b) constructed a new seismic model for central and West Antarctica by jointly inverting Rayleigh-wave phase and group velocities along with P-wave receiver functions. In this work, ambient noise tomography is used to construct Rayleigh-wave phase and group velocity dispersion maps at relatively short periods (8–40 s), and teleseismic earthquake-derived phase velocity maps at longer periods (32–*c.* 140 s) are taken from Heeszel *et al.* (2016). Comparison between the two sets of phase velocity maps at 30 s presents a difference of $-0.002 \pm 0.027 \text{ km s}^{-1}$ (<0.1% on average) for phase velocity in West and central Antarctica. This difference level is similar to the analogous comparison made in North America where seismic stations were denser, showing that high-quality ambient noise tomography can be applied to the remote continent.

These Rayleigh-wave phase and group velocity maps, together with P receiver function waveforms, were then used to construct a new 3D shear velocity model for the crust and uppermost mantle using a Bayesian Monte Carlo algorithm. Since the velocities are determined from Rayleigh waves, the maps show the velocity of vertically polarized shear waves (V_{SV}). Each Bayesian Monte Carlo inversion provides an ensemble of 1D models that fit both types of data. A final 3D model is then constructed by taking the average 1D models from the ensembles, and associated uncertainties are defined by the standard deviation of the ensembles. An example of the inversion procedure for a station in East Antarctica is shown in Figure 3, giving the fit of the preferred model to the surface-wave data (Fig. 3a) and P-wave receiver function (Fig. 3b). Incorporation of the P-wave receiver function into the inversion reduces the uncertainty in the Moho depth and crustal velocities, as shown by the comparison of the resulting structure and standard deviation (Fig. 3c, d) and prior and posterior distributions (Fig. 3f–h) for the joint inversion, as well as the inversion of surface-wave data alone. A similar Monte Carlo approach applied to Rayleigh- and Love-wave dispersions has helped to construct a 3D anisotropic model for the crust (Zhou *et al.* 2019).

The resulting 3D seismic model covers most of West Antarctica and parts of East Antarctica where there is adequate seismic station coverage for this method (Fig. 4), and extends down to the limit of good depth resolution with fundamental mode Rayleigh waves (about 200 km). The shear-wave

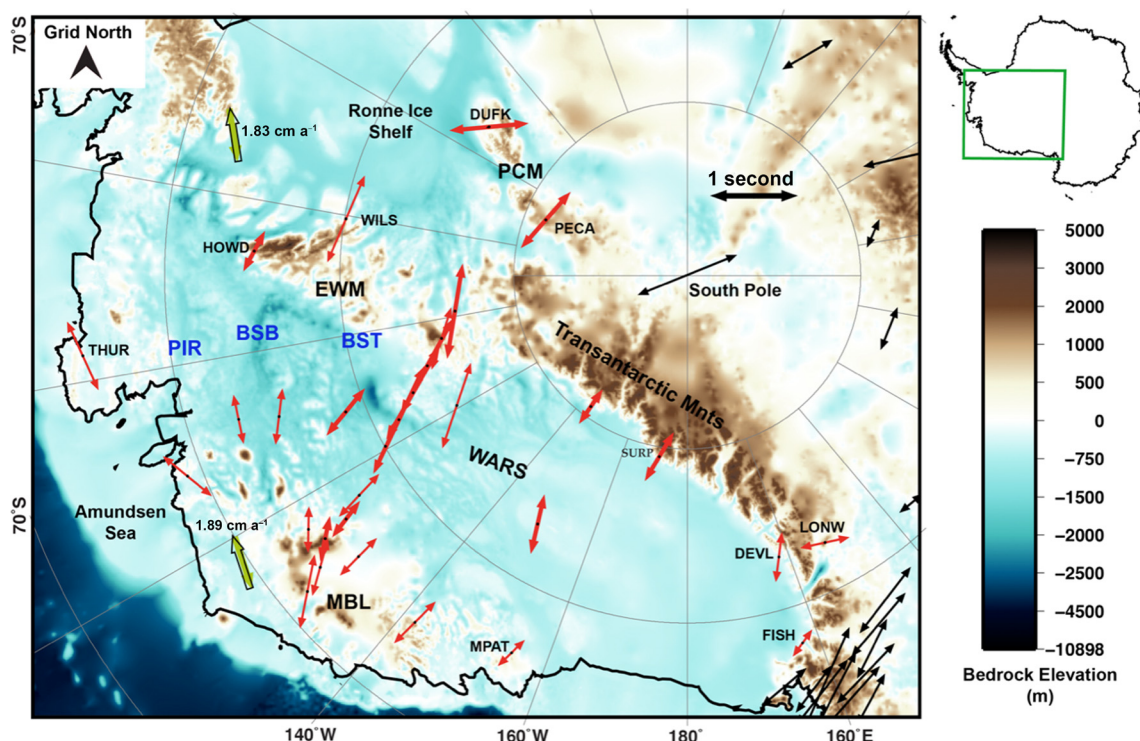


Fig. 2. Shear-wave splitting results for central West Antarctica from Accardo *et al.* (2014). The region shown is outlined in the green box on the inset map of Antarctica. Vector azimuths denote the average fast direction of splitting for arrivals at a given station. The length of the vector is proportional to the splitting time, with the splitting timescale indicated on the right. Thick red vectors represent the highest-quality measurements, thin red vectors represent the intermediate-quality measurements, and black vectors represent results assembled from other studies. Solid green arrows indicate the direction of Antarctic absolute plate motion in the hotspot reference frame. The background colour scale indicates bedrock elevation from Fretwell *et al.* (2013). Abbreviations: PIR, Pine Island Rift; BSB, Byrd Subglacial Basin; BST, Bentley Subglacial Trench; EWM, Ellsworth–Whitmore Mountains; WARS, West Antarctic Rift System.

velocity maps show a clear dichotomy of the tectonically active West Antarctica and the stable and ancient (Fig. 4). In addition, the model shows significant velocity anomalies within both West Antarctica and the central part of East Antarctica, which will be discussed later in this chapter.

Adjoint tomography

The use of 3D numerical wavefield simulations (Komatitsch and Vilotte 1998; Komatitsch and Tromp 1999) along with adjoint inversion methods (e.g. Tarantola 1984; Tromp *et al.* 2005) are proving to be a powerful tool for imaging Earth's seismological structure (e.g. Fichtner *et al.* 2009; Tape *et al.* 2010; Zhu *et al.* 2015; Bozdag *et al.* 2016). Although computationally expensive, these iterative methods are advantageous because they account for many of the complexities associated with seismic-wave propagation in a complex 3D medium, and thus allow for the accurate and efficient determination of synthetic seismograms and sensitivity kernels for all body- and surface-wave arrivals (Komatitsch and Tromp 2002a, b). The ability to use a much larger portion of the seismic wavefield, in comparison to traditional seismic imaging, to accurately map out the observational sensitivities to Earth structure, and to avoid simplifying assumptions, such as the high frequency approximation of ray theory, permits higher-fidelity seismic images over large and poorly sampled regions.

Lloyd *et al.* (2020) used this iterative adjoint tomographic inversion to seismically image the entire Antarctic continent and the surrounding southern oceans to depths of 800 km at resolutions approaching that of regional studies. The resulting radial anisotropic model (ANT-20) was determined following 20 iterations, with a 3D starting model based on the global

mantle model S362ANI (Kustowski *et al.* 2008) and a modified version of CRUST1.0 (see Lloyd *et al.* 2020). During each iteration, the model was updated to include increasingly shorter wavelength features based on travel time observations between observed and synthetic earthquake seismograms. These observations include P, S, Rayleigh and Love waves, including reflections and overtones, from 270 earthquakes recorded at 323 seismic stations, many of which are shown in Figure 1. Since ANT-20 uses both Love and Rayleigh waves to produce a radially anisotropic model, maps of velocity heterogeneity show the Voigt average shear velocity:

$$V_{\text{S-Voigt}} = \sqrt{\frac{V_{\text{SH}}^2 + 2V_{\text{SV}}^2}{3}} \quad (1)$$

Because V_{SH} is generally faster than V_{SV} in the upper mantle, the Voigt average velocities are about 1–2% faster than V_{SV} .

The high computational cost of the adjoint inversion, c. 3 million CPU hours to produce ANT-20, limits the ability to assess the model's resolution or uncertainty. Thus, evaluation of resolution relies on proxies for data density and point-spread function tests. These tests show that structures appearing in ANT-20, south of 60° S, are reliably resolved within the upper mantle and transition zone (Lloyd *et al.* 2020). The length scales of the imaged features are limited by the smoothing employed in the inversion. The lateral smoothing length ranges from c. 140 km in the upper mantle to c. 340 km in the transition zone, while the vertical smoothing length is held fixed at c. 45 km at all depths throughout the inversion. These facts, combined with comparisons to regional seismic models (e.g. Heeszel *et al.* 2016; Shen *et al.* 2018b; O'Donnell *et al.* 2019a) and other geophysical observations, indicate that

Seismic structure of the Antarctic upper mantle

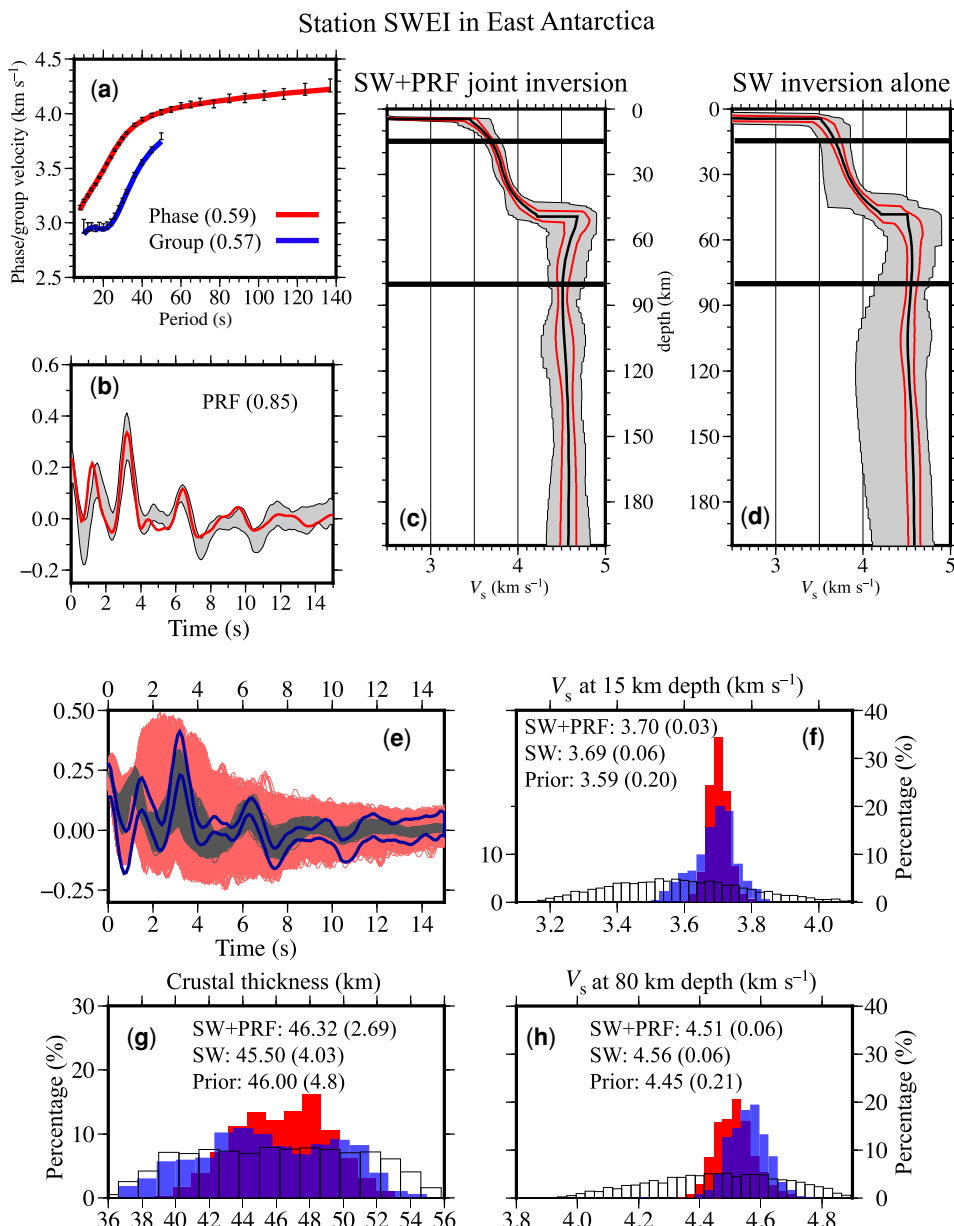


Fig. 3. Example of the joint inversion of surface-wave dispersion (SW) and P-wave receiver functions (PRF) for POLENET seismic station SWEI (Shen *et al.* 2018b). (a) and (b) Observed Rayleigh-wave phase and group velocity dispersion curves (a) and P-wave receiver function waveform (b) at station SWEI. The square root of the reduced χ^2 misfit for the preferred model is given in parentheses. (c) and (d) Results from the joint inversion of both surface-wave and receiver function data (c) and surface-wave data alone (d). Grey corridors represent the 1D seismic model ensembles, with black and red lines showing the average shear-wave velocity (V_{SV}) and the standard deviation of the 1D model. (e) Predicted receiver function waveform from models in (c) and (d) are shown as red and grey waveforms. Observed receiver functions with uncertainties are shown as two thick blue lines. (f)–(h) Prior and posterior distributions of crustal V_{SV} (15 km: f), crustal thickness (g) and mantle V_{SV} (80 km: h). Prior distributions are shown by unfilled bars and joint inversion posterior distributions are shown in red, while the surface-wave inversion posterior distribution is in blue.

ANT-20 possesses similarly high resolution across the entire Antarctic region.

Upper-mantle structure of Antarctica's tectonic regions

East Antarctica

Antarctica is divided into two very different geological subcontinents, with East Antarctica (EA) representing largely Precambrian cratonic units and West Antarctica (WA) consisting of terranes formed or tectonically modified during the Mesozoic and Cenozoic. Most of EA shows crustal thicknesses that are typical for continental cratons (Pappa *et al.* 2019b; Szwillus *et al.* 2019), whereas WA shows thinner crust similar to crustal thicknesses found in regions of extended Phanerozoic continental crust (Fig. 5). Although Archean–early Paleozoic outcrops have been sampled and mapped near the coasts and in the Transantarctic Mountains (TAMS) (Tingey 1991; Fitzsimons 2000; Goode *et al.* 2001), most of the EA interior is covered by thick ice sheets, greatly limiting our understanding of its geology. Thus, seismology and other geophysical

techniques play an outsized role in constraining the formation and geological history of EA.

Most of EA is underlain by thick continental lithosphere, as defined by strong positive velocity anomalies relative to global averages, which extends to depths of >200 km in several places (Figs 6 & 7). Similar to mantle lithosphere beneath other cratons worldwide, this continental lithosphere represents ancient, cooled mantle that may be isopycnic, and thus stable due to competing thermal and compositional buoyancy forces (Jordan 1981; Sleep 2005). The fast shear velocities arise predominantly from cold temperatures due to conductive cooling and to a lesser extent from a depleted mantle chemistry (e.g. Lee 2003; Schutt and Lesser 2006). For other continental cratons with extensive xenolith data, there is good agreement between mantle-temperature profiles inferred from mantle xenoliths and shear velocities, with both indicating thick, cold lithosphere extending to depths of >200 km (Priestley and McKenzie 2006).

Although most of EA shows seismic velocity anomalies of about 5–6% fast at depths of 75–150 km, greater variability in seismic velocity is found beneath the East Antarctic Highlands, stretching from western Dronning Maud Land to the Lambert Graben, containing several regions with mantle

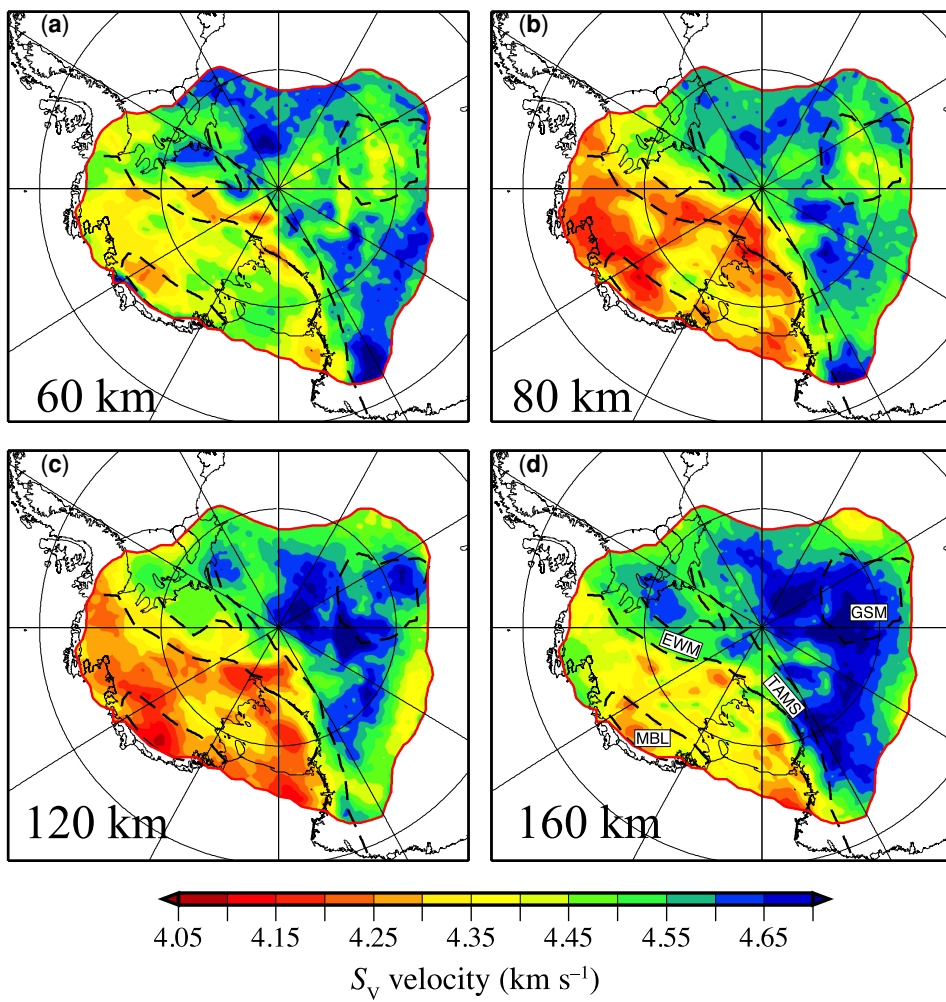


Fig. 4. Uppermost mantle V_{SV} structure from the Bayesian Monte Carlo joint inversion of surface-wave dispersion and receiver functions (Shen *et al.* 2018b). Maps show horizontal sections for depths of (a) 60 km, (b) 80 km, (c) 120 km and (d) 160 km. Dotted lines enclose the Gamburtsev Subglacial Mountains (GSM), Transantarctic Mountains (TAMS), Ellsworth–Whitmore Mountains (EWM) and Marie Byrd Land highlands (MBL).

velocities close to the global average (Fig. 6). This contrasts with several regions in central Antarctica that show fast-velocity anomalies as large as 7–8% and lithospheric thicknesses of >200 km. The variation in mantle lithospheric thickness and seismic velocity profiles allows us to understand better the distribution of lithospheric terrane ages within EA and to place constraints on the geological evolution of the continent.

The fastest seismic velocities and the thickest continental lithosphere, extending to depths of >200 km, occur along a band extending almost entirely across Antarctica 500–1000 km inboard from the TAMS (Fig. 7). Some of the thickest lithosphere is found inboard of the Miller Range in the TAMS where 3.15–3.05 Ga Nimrod Complex rocks confirm the existence of Archean-age terranes, although Mesoproterozoic units are also found in that region (Goodge and Fanning 1999, 2016), and glacial granitoid clasts show ages ranging from 2.01 to 1.06 Ga (Goodge *et al.* 2017). The thick lithosphere extends to the Shackleton Range, near the Weddell Embayment, where Paleoproterozoic rocks are preserved (Brommer *et al.* 1999; Will *et al.* 2009). Boger (2011) proposed that the ‘Shackleton’ and ‘Nimrod’ cratons are connected to late Archean ‘Gawler Craton’ rocks exposed in Australia (Swain *et al.* 2005) and along the corresponding Tierra Adélie coast of Antarctica (Oliver and Fanning 2002). The continuity of magnetic anomalies between the Antarctic and Australian coasts provides further evidence for the continuity of these cratonic regions prior to the break-up of Gondwana (Pappa and Ebbing 2021). The resulting ‘Mawson Continent’ extends entirely across EA from the coast on the Australian side to just SE of the Weddell Embayment.

The distribution of the fastest seismic velocities and thickest lithosphere in the Lloyd *et al.* (2020) seismic velocity structure correlates well with the proposed extent of the Mawson Continent, supporting the idea that this region represents the late Archean–Paleoproterozoic cratonic nucleus of Gondwana.

Thick, cold lithosphere also extends beneath the Gamburtsev Subglacial Mountains, an enigmatic highland in central Antarctica with peaks reaching to 3000 m (Ferraccioli *et al.* 2011). Surface-wave (Heeszel *et al.* 2013) and body-wave (Lloyd *et al.* 2013) tomography show that the lateral variation in mantle velocity is modest, precluding significant Mesozoic or Cenozoic mantle tectonism or rejuvenation. A systematic comparison of Rayleigh-wave phase velocity curves worldwide shows that the Gamburtsev Mountains phase velocities are best matched by Archean and Paleoproterozoic regions, suggesting that the mountains are underlain by ancient continental lithosphere (Heeszel *et al.* 2013). Shen *et al.* (2018a) found that uppermost mantle velocities (Moho–100 km depth) below the Gamburtsev Mountains are anomalously low, by 2–4%, relative to expected lithospheric craton velocities. They are also lower than surrounding regions of EA and the deeper lithosphere. A detailed discussion in Shen *et al.* (2018b) demonstrated that this anomaly is unlikely to have a thermal origin but is most likely to be the signature of a compositionally anomalous body, perhaps remnant from a continental collision in Proterozoic or early Paleozoic time (Ferraccioli *et al.* 2011; An *et al.* 2015).

The mountain elevations are largely supported by crustal thicknesses of up to about 55 km (Hansen *et al.* 2010) (see Fig. 5). Initial crustal thickening is likely to have occurred through a compressional orogeny in the Neoproterozoic–

Seismic structure of the Antarctic upper mantle

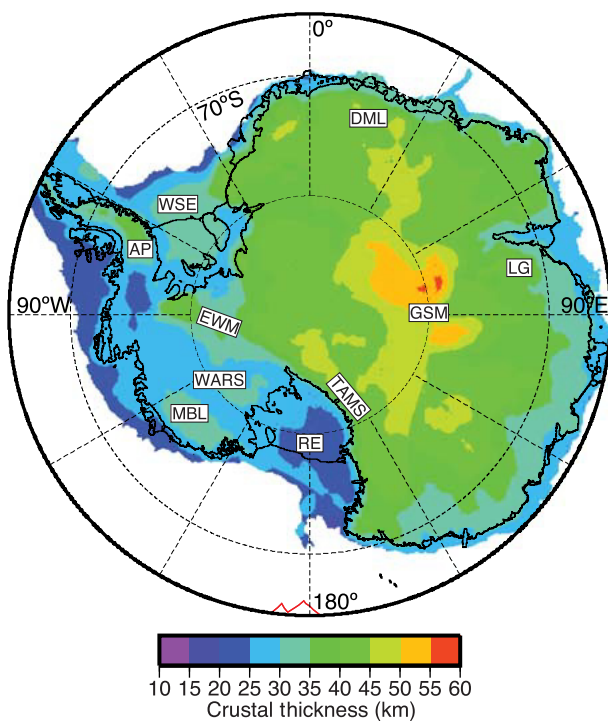


Fig. 5. Crustal thickness of Antarctica. The map is based on an inversion of seismic receiver functions and Rayleigh-wave velocities by [Shen et al. \(2018b\)](#) in West Antarctica and central Antarctica, and on GOCE satellite gravity constraints over the entire continent ([Pappa et al. 2019a](#)). The crustal thickness map based on gravity was corrected for a systematic crustal thickness offset with respect to the thicknesses derived from seismology. The resulting corrected gravity-based map was averaged with the seismic map in regions where the coverage overlapped. Abbreviations: AP, Antarctic Peninsula; EWM, Ellsworth–Whitmore Mountains; GSM, Gamburtsev Subglacial Mountains; LG, Lambert Graben; MBL, Marie Byrd Land; RE, Ross Embayment; TAMS, Transantarctic Mountains; WARS, West Antarctic Rift System; WSE, Weddell Sea Embayment.

earliest Paleozoic, which is consistent with detrital zircon studies ([van de Flierdt et al. 2008](#)), with additional uplift associated with the extension of the Lambert Graben in the late Paleozoic–early Mesozoic related to the early stages of Gondwana break-up ([Phillips and Laufer 2009; Maritati et al. 2020](#)). High elevations in this region are preserved through longer periods of geological time due to low erosion rates ([Heeszel et al. 2013; Lloyd et al. 2013](#)).

Much greater variability in lithospheric thickness is found beneath the highlands stretching from western Dronning Maud Land to the Lambert Graben ([Figs 6 & 7](#)). Thinner lithosphere, with thicknesses of the order of 100 km, is found throughout much of this region. The uppermost mantle beneath a portion of Dronning Maud Land is characterized by an absence of fast lithosphere, despite rock ages that extend from the Mesoproterozoic to the Early Paleozoic. The absence of lithosphere in a region of Paleozoic or earlier age suggests that the lithosphere has been tectonically destabilized or removed at a later time. Modest shear velocities at depths of 70–150 km suggest that the Precambrian-age lithosphere of this region has been removed, most likely by delamination ([Lloyd et al. 2020](#)). Unlike regions of Cenozoic delamination, which are characterized by low upper-mantle velocities as hot asthenosphere has replaced lithosphere (e.g. [Levander et al. 2011; Shen et al. 2018a](#)), uppermost mantle velocities in this region are near the global average. Thus, the asthenosphere that replaced the founded lithosphere has already cooled, indicating a delamination event that occurred prior to the Cenozoic. [Jacobs et al. \(2008\)](#) suggested a delamination

event occurring at c. 500 Ma to explain the late-tectonic granitoid intrusions found in Dronning Maud Land, consistent with the seismic structure.

The Lambert Graben and other neighbouring regions to the west represent an ancient terrane, with basement rocks ranging from Archean to earliest Paleozoic ([Fitzsimons 2000](#)), which also lacks thick continental lithosphere ([Figs 6 & 7](#)). Seismic structures in this region show that high lithospheric velocities are limited to depths of <75–100 km, suggesting the existence of thin lithosphere, in contrast to surrounding regions where high velocities extend to c. 200 km ([Lloyd et al. 2020](#)). The Lambert Graben and corresponding rift structures in India developed during Carboniferous–early Cretaceous extension associated with the break-up of Gondwana ([Phillips and Laufer 2009](#)). Xenolith suites from the Lambert Graben indicate a transition from a relatively cold to a warmer geotherm that is likely to have occurred during the late Paleozoic early rifting stages and Mesozoic formation of the graben ([Foley et al. 2006, 2021](#)). Thus, mantle geodynamic processes associated with this extension and rifting heated and destabilized the existing Precambrian lithosphere, thinning or removing it.

Transantarctic Mountains and adjacent rifts

The TAMS are traditionally viewed as the tectonic boundary between the thick Precambrian cratonic lithosphere of EA and the Phanerozoic lithosphere domains of WA, although there is some evidence that crust of EA affinity extends to the middle of the Ross Sea ([Tinto et al. 2019](#)). The 4000 km-long mountain range with peaks of up to c. 4000 m exhibits strong along-strike variations, varying from a narrow, rift-shoulder-like orogeny in the central TAMS to broad, 400 km-wide, plateau-like elevated areas in the southernmost and northernmost segments. These variations in topography reflect a complicated history of tectonism along the TAMS, and correlate with changes in the underlying upper-mantle structure, as imaged in the latest seismic models ([Shen et al. 2018a; Lloyd et al. 2020](#)).

Seismic tomography reveals a band of slow velocities extending from the Macquarie Triple Junction, through the volcanic Balleny Islands, the extinct Adare Trough spreading centre and along the front of the TAMS ([Fig. 6](#)). This pattern suggests that the TAMS and Terror Rift are part of a larger tectonic system linked to mantle geodynamic processes, stretching from the mid-ocean ridge to the southern TAMS. The Adare Trough, located just north of the Ross Embayment near the northern terminus of the TAMS, displays magnetic anomalies resulting from seafloor spreading from 46 to 26 Ma ([Granot et al. 2013](#)), with slow spreading continuing to 11 Ma and evidence of extensional faulting up to the present ([Granot and Dyment 2018](#)). The western side of the Ross Embayment accommodated almost 100 km of extension from 40 to 26 Ma associated with plate motion between EA and WA ([Wilson and Luyendyk 2009; Granot et al. 2013; Davey et al. 2016](#)). Very slow extension and rift sedimentation occurred since that time along the Terror Rift, which parallels the TAMS along the western Ross Embayment ([Fielding et al. 2008; Martin and Cooper 2010; Granot and Dyment 2018](#)). The slow wave speeds show that the upper mantle retains warm uppermost mantle temperatures caused by an extensional tectonic environment despite the fact that tectonic motion along this boundary has largely ceased, as shown by the absence of resolvable motion in GPS surveys (T. Wilson pers. comm.). Anomalously warm upper-mantle temperatures are also indicated for this region by mantle xenolith studies (e.g. [Martin et al. 2021a](#)).

The northern section of the TAMS mostly constitutes the highlands of northern Victoria Land (NVL). Surface- and

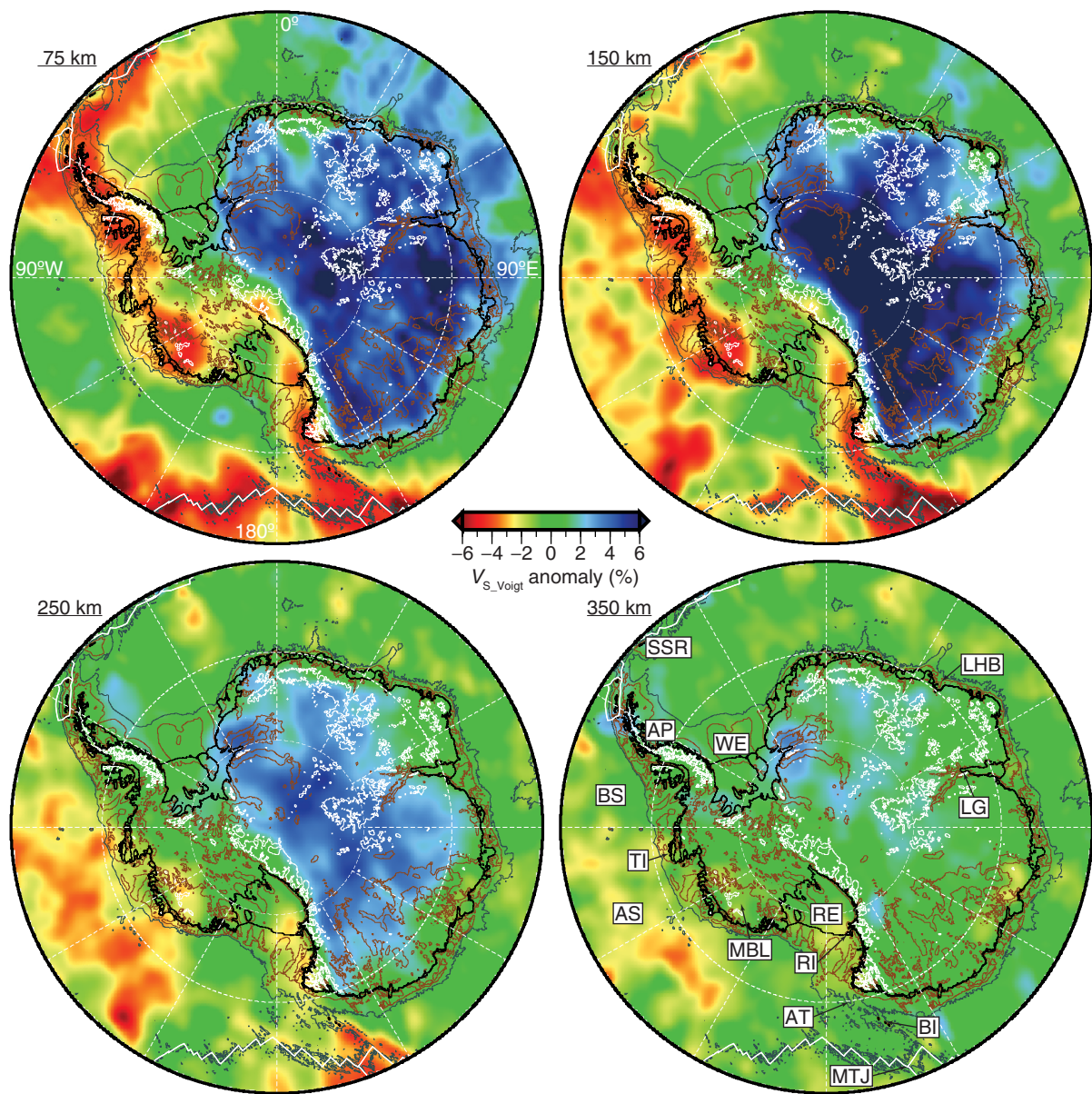


Fig. 6. Tomographic images of the shear-wave velocity structure of seismic model ANT-20 at depths of 75, 150, 250 and 350 km from Lloyd *et al.* (2020). Bathymetry and bedrock topography contours for 1000 m (thin white line) and -500 m (thin brown line), as well as -2500 m (thin dark grey line) in the oceans are also shown (Fretwell *et al.* 2013). Abbreviations: AT, Adare Trough; AS, Amundsen Sea; AP, Antarctic Peninsula; BI, Balleny Islands; BS, Bellingshausen Sea; LG, Lambert Graben; LHB, Lützow-Holm Bay; MTJ, Macquarie Triple Junction; MBL, Marie Byrd Land; RE, Ross Embayment; RI, Ross Island; SSR, South Scotia Ridge; TI, Thurston Island; WE, Weddell Embayment.

body-wave tomography using a regional temporary seismic array revealed that a slow-velocity anomaly in the upper mantle between Moho and 150 km depth is located near the coastline of NVL (Hansen *et al.* 2015; Graw *et al.* 2016; Brenn *et al.* 2017). The continental-scale model from Lloyd *et al.* (2020) shows a large slow-velocity region in the uppermost mantle beneath the high elevations of northernmost Victoria Land and the adjacent areas of the Ross Embayment that connect the Balleny Islands to the north and Ross Island to the south (Fig. 6). This extended region of low velocity in the upper mantle implies a strong thermal contribution to the uplift of NVL.

Detailed body- and surface-wave tomography using temporary seismic stations shows a sharp boundary between slow and fast upper mantle, near the crest of the TAMS near Ross Island (Lawrence *et al.* 2006a; Watson *et al.* 2006; Brenn *et al.* 2017; Shen *et al.* 2018b; White-Gaynor *et al.* 2019). There is also a sharp boundary along the TAMS between

low mantle seismic attenuation in EA and high mantle attenuation beneath Ross Island and the Terror Rift (Lawrence *et al.* 2006b). The slow wave speeds in this region are consistent with the general absence of lithosphere and the high uppermantle temperatures expected beneath a recently extending rift zone with a small amount of continuing decompression melting.

Active volcanism along the western coast of the Ross Embayment, mostly over the past 10 myr, extends from the northernmost tip of the coastline to just south of Ross Island (Kyle 1990). A mantle plume origin has been proposed for Mount Erebus, on Ross Island, based largely on petrological and geochemical data (Kyle *et al.* 1992; Phillips *et al.* 2018), although other studies associate the volcanism with mantle metasomatism from the long subduction history in this region (Day *et al.* 2019; Martin *et al.* 2021b). Adjoint tomography shows that Ross Island is underlain by a prominent slow-velocity anomaly extending down to the 410 km

Seismic structure of the Antarctic upper mantle

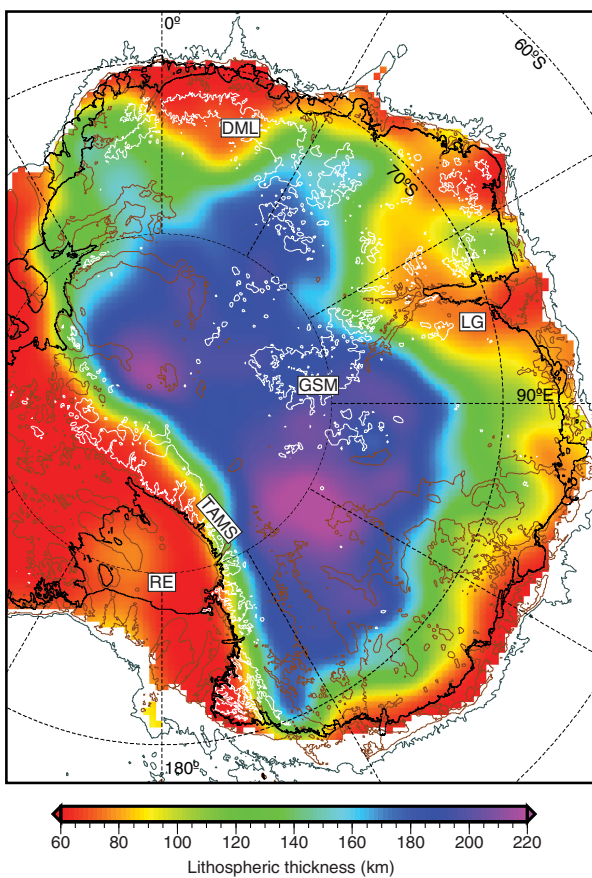


Fig. 7. Lithospheric thickness of East Antarctica based on the ANT-20 seismic model (Lloyd *et al.* 2020). Lithospheric thickness was calculated from velocity profiles assuming that the bottom of the lithosphere is located at the depth of the maximum negative velocity gradient above the low-velocity zone (van der Lee 2002). Geographical labels are the same as in Figure 5.

discontinuity but anomalies beneath this are low amplitude and indistinct (Lloyd *et al.* 2020). P-wave travel-time tomography also shows prominent upper-mantle slow-velocity anomalies but the anomalies diverge laterally in the transition zone (Hansen *et al.* 2014; White-Gaynor *et al.* 2019). This does not necessarily eliminate the plume model, since geodynamical modelling suggests that plumes may be highly tilted in the mid-mantle (Bredow and Steinberger 2021). Emry *et al.* (2020), using receiver functions, found that the mantle transition zone was anomalously thin near Mount Erebus and along the adjacent TAMS, suggesting a warm thermal anomaly in the transition zone. French and Romanowicz (2015), in a global tomographic study, showed little anomaly in the transition zone, a significant slow anomaly at depths of 800–1200 km and no anomalies in the lower mantle (Phillips *et al.* 2018). Thus, it is clear that the region is underlain by a significant thermal anomaly in the upper mantle but the existence of a classic mantle plume arising near the core–mantle boundary remains uncertain.

The southern section of the TAMS shows some unusual characteristics compared with other sections of the TAM. First, unlike the nearby central TAMS where the exposed high mountains are only c. 100 km wide, the southern TAMS has a plateau-like elevated region extending into EA for c. 400 km. Secondly, unlike the central and northern TAMS where volcanic rocks are only found on the West Antarctic Rift (WARS) side of the high mountains, Miocene-age (c. 20–15 Ma) volcanics at Sheridan Bluff and Mount Early (Fig. 8) are all located on the EA side of the peaks

(Stump *et al.* 1980). Notably, recently found volcanic rocks in glacial deposits show ages of 25–17 Ma and can be traced to a magnetic anomaly 400 km into EA (Licht *et al.* 2018). Both the topographic and volcanic features pose difficulties to the flexural rift-shoulder mountain model as its support (see Paxman 2021 for a discussion of uplift mechanisms).

Using surface-wave tomography, Heeszel *et al.* (2016) found a slow uppermost mantle beneath the southern TAMS region. They hypothesized that the slow anomaly was either due to the reheating from the WARS activity related to the Terror Rift to the north, or evidence of a Cenozoic lithospheric delamination or destruction event. Shen *et al.* (2018a) further improved the images by combining data from Heeszel *et al.* (2016) together with short-period surface-wave velocity maps from ambient noise and receiver functions. The updated images show a low-velocity zone beneath the southern TAMS in the uppermost mantle (Fig. 8) on top of a dipping high-velocity zone (Fig. 9). They suggested that the deeper high-velocity zone represents a foundering lithosphere and the LVZ represents an upwelling asthenosphere, and the system is best interpreted by a lithosphere removal model (Shen *et al.* 2018a). Beneath the Thiel Mountains and Whitmore Mountains, the same study also identified an additional low seismic anomaly in the uppermost mantle, indicative of a thermal origin for these elevated areas in WA.

Although Shen *et al.* (2018a) showed that the lithosphere has been removed in the southern TAMS region and provided an estimate of the contribution to uplift from the mantle thermal effect due to the lithosphere removal, it is also clear that the TAMS is complicated and significant along-strike variation exists. Proposed uplift mechanisms for the TAMS include flexural uplift (ten Brink *et al.* 1997; Yamasaki *et al.* 2008; Wannamaker *et al.* 2017), thermal mantle support (Lawrence *et al.* 2006c; Brenn *et al.* 2017), and crustal thickness and density variations (Bialas *et al.* 2007; Huerta 2007). As an

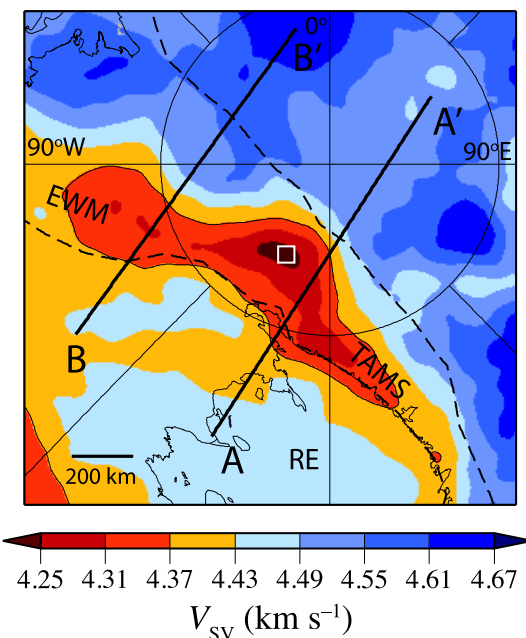


Fig. 8. Average V_s in the uppermost 50 km of the mantle beneath central Antarctica, showing the absence of cold, fast mantle lithosphere beneath the Transantarctic Mountains (Shen *et al.* 2018a). Black lines indicate the locations of the two vertical profiles shown in Figure 9. A small open box marks the approximate location of the Mount Early and Sheridan Bluff volcanism. The Ellsworth–Whitmore Mountains (EWM), the Transantarctic Mountains (TAMS) and the Ross Embayment (RE) are labelled. Lines A–A' and B–B' denote the location of the cross-sections shown in Figure 9.

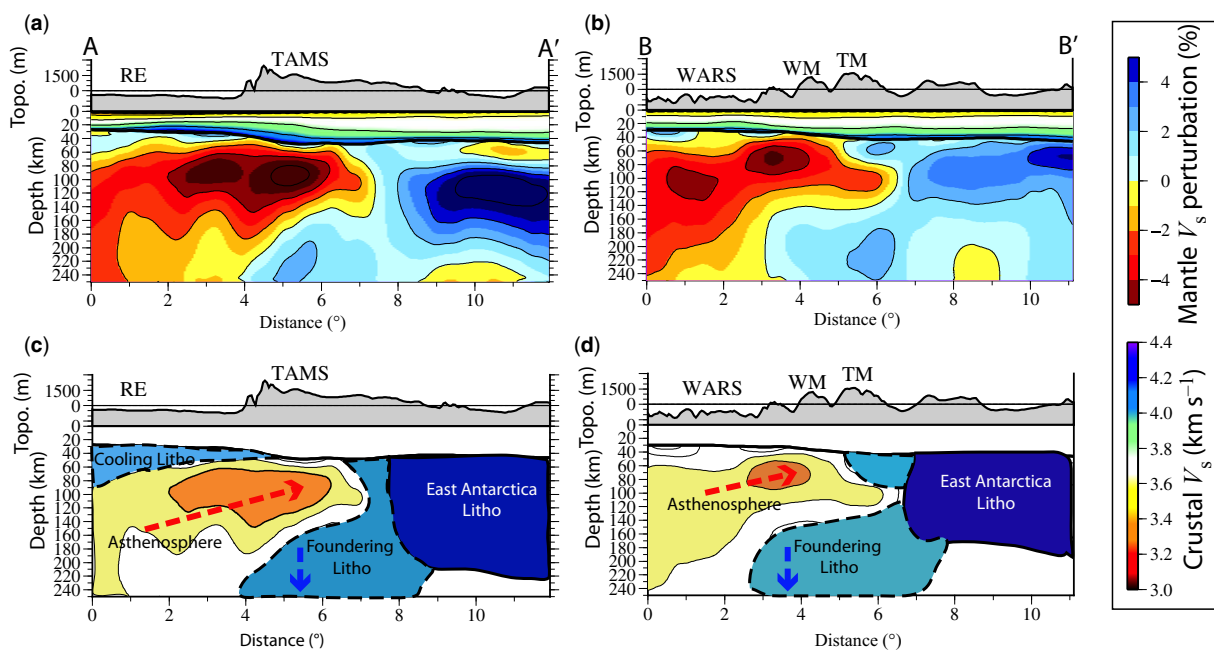


Fig. 9. Cross-sections beneath the southern Transantarctic Mountains and Whitmore Mountains along lines A–A' and B–B' in Figure 8, from Shen *et al.* (2018a). (a) and (b) show V_{SV} , and (c) and (d) show the corresponding interpretation. The elevation of the solid Earth surface in metres is shown above each plot. V_{SV} in the crust is plotted as an absolute value, and V_{SV} in the mantle is plotted as the per cent perturbation relative to the averaged 1D V_{SV} structure of the study region. Geographical features are marked by abbreviations: RE, Ross Embayment; TAMS, Transantarctic Mountains; TM, Thiel Mountains; WARS, West Antarctic Rift System; WM, Whitmore Mountains.

example of along-strike variation, a recent magnetotelluric (MT) study by Wannamaker *et al.* (2017) showed that in the central TAM, cratonic lithosphere extends nearly up to the TAMS range front. Cantilevered flexural uplift appears to be the preferred uplift mechanism and the thermal contribution from the mantle seems smaller in this region. These differences between the southern and central TAMS are consistent with the range morphology, in which the southern TAMS form a large plateau area, whereas the central TAMS form a much narrower mountain range. Indeed, such structural and morphological variability is evident along the full length of the TAMS (Shen *et al.* 2018a; Lloyd *et al.* 2020).

West Antarctica

The upper-mantle structure of WA is broadly similar to other regions worldwide that have experienced Mesozoic and Cenozoic tectonic activity, such as western North America. This structure includes shallow Moho depth (Fig. 5), thin lithosphere and slow upper-mantle shear wave velocities in many places (Fig. 6). These characteristics are consistent with the geological history of WA, which includes rifting in the Weddell Sea Embayment (Jordan *et al.* 2017) as well as the rotation and translation of the Ellsworth–Whitmore Mountain block during the Jurassic (Grunow *et al.* 1987), and Cretaceous extension between the WA crustal block and Zealandia (e.g. Siddoway 2008; Wobbe *et al.* 2012). The latter events culminated in the regional cessation of subduction along the margin of Marie Byrd Land. However, subduction continued from Thurston Island to the Antarctic Peninsula, where it gradually ceased from south to north during the Cenozoic (Eagles *et al.* 2004). The extended continental crust of the WARS underwent further episodes of focused extension during the Cenozoic (Granot *et al.* 2013; Davey *et al.* 2016).

The eastern Ross Embayment, central WA and the Weddell Sea show modest upper-mantle velocity anomalies, with velocities about 1–2% slower than the global average

reference velocity (Figs 4, 6, 10 & 11). Mantle seismic velocities increase eastwards across the Ross Embayment, consistent with the increase in lithospheric age from the late Cenozoic rifting in the western Ross Embayment (Fielding *et al.* 2008) to early Cenozoic and Cretaceous lithosphere in the east (Wilson and Luyendyk 2009). Although aerogeophysical evidence suggests that the boundary between crust of EA and WA affinities occurs in the middle of the Ross Embayment (Tinto *et al.* 2019), from a seismic structure and tectonics standpoint the boundary occurs along the TAMS. Detailed surface-wave results show that the structure of the WARS consists of higher-velocity lithospheric mantle extending to depths of about 70–80 km, with lower velocities beneath (Heeszel *et al.* 2016; O'Donnell *et al.* 2017; Shen *et al.* 2018b), consistent with cooling since the major extensional episodes during the Mesozoic and early Cenozoic (Siddoway 2008; Granot *et al.* 2013). Some smaller regions show lower velocities, possibly delineating the locus of limited late Cenozoic extension (Lloyd *et al.* 2015). The Weddell Sea and areas beneath the Ronne Ice Shelf show upper-mantle velocities that are intermediate between the fast EA lithosphere and the lower velocities in other regions of WA (Figs 6 & 11). This is consistent with the age of the lithosphere in this region, dating to the Mesozoic opening of Gondwana (Jordan *et al.* 2013; 2017).

Shear-wave splitting measurements indicate large shear-wave splitting times (>1 s) in the southern WARS (Fig. 2). The splitting measurements show very consistent fast directions approximately perpendicular to the strike of the nearby Whitmore Mountains and other topographical features, and parallel to likely extension directions for the WARS opening. This strong upper-mantle azimuthal anisotropy is interpreted as resulting from lattice-preferred orientation induced by asthenospheric mantle strain associated with Cenozoic extension of the WARS (Accardo *et al.* 2014).

Marie Byrd Land (MBL), an elevated volcanic dome with 18 major subaerial shield and stratovolcanoes (LeMasurier and Rex 1989), is underlain by low mantle velocities (Figs 6

Seismic structure of the Antarctic upper mantle

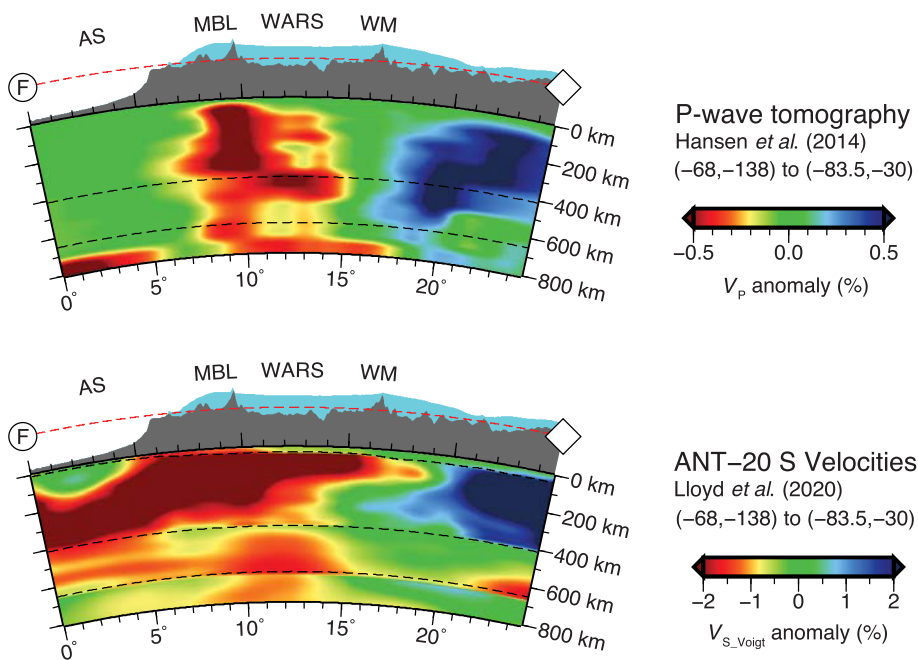


Fig. 10. Comparison of P-wave travel-time tomography (Hansen *et al.* 2014) with adjoint waveform tomography (Lloyd *et al.* 2020) results for a profile across the Amundsen Sea (AS), Marie Byrd Land (MBL), the West Antarctic Rift System (WARS) and the Whitmore Mountains (WM), along line F in Figure 11. The images show generally similar features in areas below the continent with good P-wave ray-path coverage (below MBL and East Antarctica) but anomalies are missing from the P-wave model in regions with little ray-path coverage, such as the Amundsen Sea coast. Both models show that slow-velocity anomalies beneath the Marie Byrd Land dome continue into the lower mantle, consistent with a mantle plume origin for the topography and volcanism.

& 10). Late Quaternary alkaline volcanism at Mount Berlin and Mount Takahae (Wilch *et al.* 1999), and an inferred subglacial magmatic system near Mount Waesche (Lough *et al.* 2013), demonstrate current volcanic activity. The crustal thickness of about 30–33 km (Fig. 5) is somewhat greater

than the surrounding regions (*c.* 25–28 km) but this is not sufficient to explain the elevated topography, suggesting that the elevation is partially supported by a low-density thermal anomaly in the uppermost mantle (Chaput *et al.* 2014; Shen *et al.* 2018a). Several previous studies have proposed a mantle

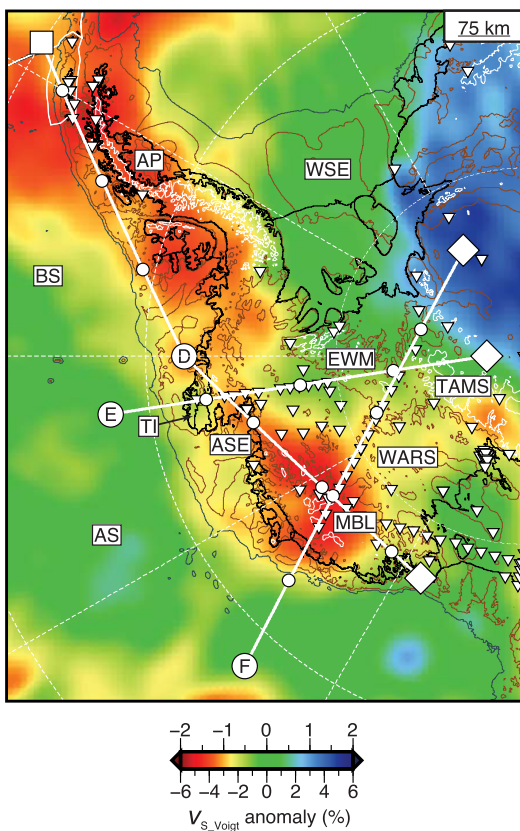
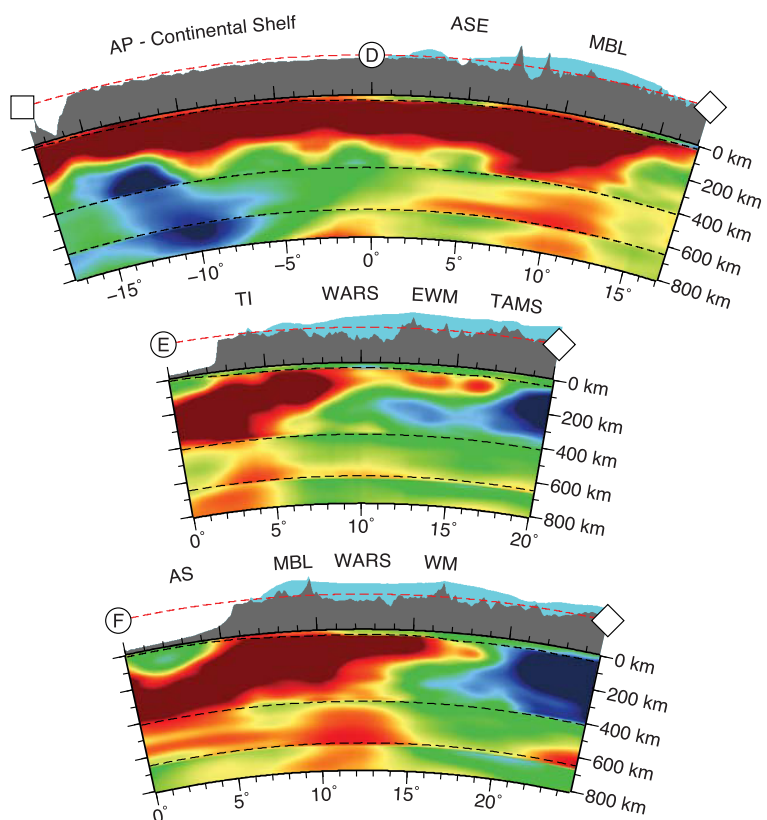


Fig. 11. Images of shear-wave speed structure beneath West Antarctica at 75 km depth and along profiles D, E and F from Lloyd *et al.* (2020). Horizontal and vertical slices have a shear-wave speed range of ± 6 and $\pm 2\%$, respectively. The horizontal slice depicts broadband seismic stations, wave-speed anomalies, bathymetry and topography as in Figure 6. Abbreviations: AS, Amundsen Sea; ASE, Amundsen Sea Embayment; AP, Antarctic Peninsula; BS, Bellingshausen Sea; EWM, Ellsworth–Whitmore Mountains; MBL, Marie Byrd Land; TAMS, Transantarctic Mountains; TI, Thurston Island; WARS, West Antarctic Rift System; WSE, Weddell Sea Embayment; WM, Whitmore Mountains.



plume origin for the MBL dome, based on the elevated topography and volcano chemistry and petrology (Hole and LeMasurier 1994; LeMasurier and Landis 1996; Behrendt 1999; Panter *et al.* 2000). Subaerial volcanic peaks are located along linear arrays, in many cases with age progressions, but directions of propagation are not consistent between difference lines, suggesting that the linear trends may be controlled by pre-existing fractures (LeMasurier and Rex 1989; Paulsen and Wilson 2010) rather than relative motion between the Antarctic Plate and the mantle plume. As an alternative to the mantle plume model, Finn *et al.* (2005) proposed that much of the volcanism of WA results from the volatile-enhanced melting of metasomatized lithosphere formed during Mesozoic subduction along this margin.

Both body-wave (Hansen *et al.* 2014; Lloyd *et al.* 2015) and surface-wave (Heeszel *et al.* 2016; Shen *et al.* 2018b) tomography studies show low velocities in the upper mantle beneath the MBL dome. The surface-wave results show the existence of a higher-velocity mantle lithosphere to depths of 60–80 km, underlain by lower seismic velocities. Methods with good sensitivity to mid-mantle depths generally show low-velocity anomalies beneath the MBL dome in the transition zone and upper part of the lower mantle. Figure 10 compares the results from P-wave tomography (Hansen *et al.* 2014) and adjoint tomography (Lloyd *et al.* 2020), with both results showing low velocities in the mid-mantle beneath the MBL dome. The P-wave tomography has almost no resolution of the coastal and oceanic regions due to a lack of seismic stations resulting in poor ray-path coverage but the adjoint tomography, which has good resolution, shows that the low upper-mantle velocities extend past the MBL coastline to a low-velocity anomaly at depths of 150–350 km beneath the Amundsen Sea.

The tomography results are consistent with a thermal plume extending at least from the mid-mantle to the surface beneath MBL. The velocity anomalies are most easily interpreted in terms of warmer mantle temperatures, as the effects of water on seismic velocities are uncertain and recent laboratory results suggest that water has an insignificant effect on upper-mantle seismic velocities (Cline *et al.* 2018). The magnitude of the shear velocity anomaly is consistent with a 150°C upper-mantle thermal anomaly, which can explain the excess topography (Lloyd *et al.* 2015). The continuity of the slow-velocity anomalies from depths of 80 to 800 km is highly suggestive of a mantle plume originating from the mid-mantle or deeper, which is consistent with geochemical evidence (e.g. Panter *et al.* 2000; Handler *et al.* 2021). However, the connection between the MBL anomaly and the offshore anomaly, as well as the diverse geographical trends of the volcanic lines, suggest the possibility of a more complicated geodynamical situation than indicated by the classical simple vertical plume model. Simulations of mantle plumes in global mantle-flow models suggest that plumes originating at the edge of the Pacific Large Low Shear Velocity Province (LLSVP) at the core–mantle boundary beneath the South Pacific would be tilted southwards by the large-scale mantle flow pattern, possibly explaining the MBL and offshore seismic anomalies (Bredow and Steinberger 2021).

Slow upper-mantle velocity anomalies extend along the coast from MBL through the Amundsen Sea Embayment and northwards to the tip of the Antarctic Peninsula (Fig. 11). Along the MBL and Amundsen Sea coastlines, slow velocities extend from the bottom of the thin lithosphere (70 km) to about 200 km depth, beneath late Pleistocene–recent volcanoes such as Mount Siple in MBL (Wilch *et al.* 1999) and Mount Hudson (Corr and Vaughan 2008) near the Amundsen Sea Embayment. The anomalies deepen to 150–300 km depth offshore beneath 90 Ma oceanic lithosphere formed during the separation of Zealandia from

Antarctica (Eagles *et al.* 2004), where an extensive shallow bathymetric anomaly is found (Wobbe *et al.* 2014). The seismic and bathymetric anomalies may result from warm upper mantle near the region where spreading originated between Zealandia and Antarctica, in which the initiation of spreading has been attributed to a mantle plume (Weaver *et al.* 1994). The presence of low-viscosity hydrous mantle material resulting from the long-lived Mesozoic subduction zone that preceded the rifting along the northern Antarctic margin may also play a role (Finn *et al.* 2005; Sutherland *et al.* 2010).

Slow seismic anomalies beneath the Antarctic Peninsula are limited to depths of <200 km, and are underlain by fast velocities, in contrast to MBL and the Amundsen Sea regions (Fig. 11). This region was the site of subduction of the Phoenix Plate beneath Antarctica during the Mesozoic, with subduction ending from south to north during the Cenozoic as the Phoenix–Antarctic spreading centre was subducted (Eagles *et al.* 2004). The fast velocities found in the transition zone beneath the northern peninsula may represent the remnants of the subducted Phoenix slab. As the subducting ridge traversed northwards along the peninsula, it formed a slab window in its wake. Slab windows are generally accompanied by erosion of the overriding plate lithosphere and its replacement with hot upwelling asthenosphere (Groome and Thorkelson 2009). We interpret the slow seismic velocities extending along the entire length of the western margin of the peninsula as due to the effects of the slab window, consistent with the location and limited depth extent of the anomalies.

The slow mantle velocities beneath MBL, the Amundsen Sea Embayment and the Antarctic Peninsula imply warm upper-mantle temperatures, with important implications for ice sheet models and projections of the future of the Antarctic ice sheet. Heat-flow estimates, based on the seismic structure, show relatively high geothermal heat flux in these regions (Shen *et al.* 2020), influencing water production and drag at the base of the ice sheet (Pollard *et al.* 2005; Pattyn 2010). Warm mantle temperatures also imply low mantle viscosity, which predicts short glacial isostatic adjustment timescales that may have important influences on the evolution of the Antarctic ice sheet (Gomez *et al.* 2015; Whitehouse *et al.* 2019). The relationship between Antarctic seismic structure, mantle viscosity and glacial isostatic adjustment is discussed further in Ivins *et al.* (In press).

Conclusions and prospects for future work

The deployment of numerous seismic stations and the development of new seismic analysis tools over the last two decades have led to great improvements in our knowledge of the upper-mantle structure beneath Antarctica. Analysis of empirical Green's functions from ambient noise correlation allows much better resolution of surface-wave dispersion curves at short periods. Bayesian Monte Carlo inversion methods can be used to determine the structure that best fits constraints from multiple types of seismic data, and also provide uncertainty estimates. Adjoint inversion methods, combined with numerical calculations of full waveform synthetic seismograms in 3D structures, allows the determination of higher-resolution structure models of the entire Antarctic continent and surrounding regions throughout the upper mantle and transition zone.

Seismic structure models calculated with these methods now have sufficient resolution to provide important insights into the geological history of the continent. EA shows thick continental mantle lithosphere similar to Archean and Early Proterozoic terranes on other continents. The fast shear velocities of the lithosphere down to >200 km depth are interpreted

Seismic structure of the Antarctic upper mantle

as resulting from cold mantle temperatures, and to a lesser extent from chemical depletion, based on studies from other cratonic regions. The deepest and largest lithospheric velocity anomalies occur along a band extending almost entirely across Antarctica 500–1000 km inboard from the TAM, probably representing a ‘Mawson Continent’ that formed the core of ancient cratonic lithosphere around which other terranes accreted. Some other regions of EA, notably the Dronning Maud Land highlands and the Lambert Graben region, show much thinner lithosphere, indicating thermal modification of the lithosphere during the Phanerozoic.

The TAMS front represents a major boundary in the mantle between thick cratonic lithosphere in EA and much thinner lithosphere in WA. In the Ross Embayment region, it is flanked by the late Cenozoic rifts, which are underlain by an extensive low-velocity upper-mantle anomaly extending from the mid-ocean ridges north of Antarctica to the southern TAM. This velocity anomaly results from warm mantle along the trace of the rift, which persists even though extension has now apparently ceased. The TAMS show major structural variations along-strike, with the broad southern TAMS underlain at shallow mantle depths by low seismic velocities indicating an absence of lithospheric mantle, consistent with uplift as a result of lithospheric removal. In contrast, the much narrower central TAMS is underlain by a sharp boundary between slow WA and fast EA mantle, consistent with classical rift-shoulder or flexural uplift models.

The upper-mantle seismic structure of WA is dominated by large slow-velocity anomalies beneath central MBL, and along the Pacific coastline from MBL through the Antarctic Peninsula. The central MBL anomaly extends through the transition zone, and may represent the thermal anomaly resulting from a mantle plume. Slow velocities beneath the Amundsen Sea coast link to deeper anomalies offshore, suggesting a connection with deeper mantle processes to the north. Slow anomalies beneath the Antarctic Peninsula are limited to depths <200 km, and are likely to represent thermal anomalies resulting from the erosion of continental lithosphere and replacement by warm mantle during subduction of the Antarctic–Phoenix spreading centre.

Continuing work over the next decade should result in higher-resolution seismic images of the mantle structure due to improvements in both data collection and seismic analysis. Technological improvements should permit the deployment of denser arrays of seismic stations, as well as deployment of stations in regions without previous instrumentation. The development of much smaller and lighter autonomous seismic stations with more reliable power supplies should facilitate deployment in remote parts of the continent. Better and lower-cost satellite communications should allow real-time transmission of seismic data from remote sites, and should also reduce the cost of operation by reducing the need for maintenance visits. An international effort is needed to instrument the vast regions of EA that are so far without any seismograph deployments.

Improvements in data analysis will also allow advances to take place using existing data. Surface-wave data can be analysed to yield better constraints on anisotropy. Combined analysis of Love and Rayleigh waves will yield estimates on the variations in radial seismic anisotropy, the difference between vertically and horizontally polarized shear waves (O’Donnell *et al.* 2019b; Zhou *et al.* 2019). Analysis of Rayleigh-wave phase velocities for azimuthal anisotropy will allow resolution of the depth distribution of azimuthal anisotropy, which is poorly constrained by SKS analysis. The resulting maps of the lateral and depth distribution of azimuthal anisotropy will provide important constraints on the distribution and orientation of mantle fabric due to either past tectonic processes or to current mantle deformation and flow. Improved

techniques will also increase the resolution of isotropic structural variations. Double difference tomography, which uses the differences in waveforms from the same earthquake recorded at different seismic stations, will improve resolution on the Antarctic continent by localizing the structure kernels in the vicinity of the stations (Yuan *et al.* 2016). The incorporation of Green’s functions from ambient noise cross-correlation into adjoint tomography will also increase resolution (Chen *et al.* 2014; Liu *et al.* 2017). With the continued improvement of datasets and analysis methods, future seismic studies of the Antarctic mantle will provide important new insights into the geological history and current geodynamic processes of Antarctica.

Acknowledgements We thank the many individuals and organizations who have helped with the installation and maintenance of Antarctic seismic stations through the years. The seismic instruments were provided by the Incorporated Research Institutions for Seismology (IRIS) through the PASSCAL Polar Support Services. We thank Anya Reading, Fausto Ferraccioli, Adam Martin and Wouter van der Wal for helpful comments on an earlier draft.

The portable instrumentation and data management facilities of the IRIS Consortium are supported by the National Science Foundation’s Seismological Facilities for the Advancement of Geoscience (SAGE) Award under Cooperative Support Agreement OPP-1851037.

Author contributions DAW: conceptualization (lead), funding acquisition (lead), investigation (equal), methodology (equal), project administration (lead), resources (lead), software (supporting), supervision (lead), validation (equal), visualization (equal), writing – original draft (lead), writing – review & editing (lead); WS: conceptualization (supporting), data curation (lead), formal analysis (lead), funding acquisition (supporting), investigation (equal), methodology (equal), project administration (supporting), resources (supporting), software (lead), validation (equal), visualization (equal), writing – original draft (supporting), writing – review & editing (supporting); AJL: conceptualization (supporting), data curation (lead), formal analysis (lead), funding acquisition (supporting), investigation (equal), methodology (equal), project administration (supporting), resources (supporting), software (lead), validation (equal), visualization (lead), writing – original draft (supporting), writing – review & editing (supporting).

Funding This work was funded by the United States National Science Foundation with grants PLR-1246712, OPP-1744883, OPP-1744889 and OPP-1945693 awarded to D.A. Wiens, and grant OPP-1945856 awarded to W. Shen.

Data availability Original data can be obtained from the IRIS Data Management Center (<http://ds.iris.edu/ds/nodes/dmc/data/>). The shear-wave velocity structures of the Bayesian Monte-Carlo and adjoint ANT-20 models can be obtained through the Incorporated Research Institutions for Seismology (IRIS) Earth Model Collaboration (<http://ds.iris.edu/ds/products/emc/>).

References

- Accardo, N.J., Wiens, D.A. *et al.* 2014. Upper mantle seismic anisotropy beneath the West Antarctic Rift System and surrounding region from shear wave splitting analysis. *Geophysical Journal International*, **198**, 414–429, <https://doi.org/10.1093/gji/ggu117>
- Ammon, C. 1991. The isolation of receiver effects from teleseismic P waveforms. *Bulletin of the Seismological Society of America*, **81**, 2504–2510.

- An, M., Wiens, D.A. *et al.* 2015. S-velocity model and inferred Moho topography beneath the Antarctic Plate from Rayleigh waves. *Journal of Geophysical Research: Solid Earth*, **120**, 359–383, <https://doi.org/10.1002/2014JB011332>
- Anandakrishnan, A., Voigt, D.E., Burkett, P.G. and Henry, R. 2000. Deployment of a broadband seismic network in west Antarctica. *Geophysical Research Letters*, **27**, 2053–2056, <https://doi.org/10.1029/1999GL011189>
- Baker, M.G., Aster, R.C. *et al.* 2019. Seasonal and spatial variations in the ocean-coupled ambient wavefield of the Ross Ice Shelf. *Journal of Glaciology*, **65**, 912–925, <https://doi.org/10.1017/jog.2019.64>
- Bannister, S., Yu, J., Leitner, B. and Kennett, B.L.N. 2003. Variations in crustal structure across the transition from West to East Antarctica, Southern Victoria Land. *Geophysical Journal International*, **155**, 870–884, <https://doi.org/10.1111/j.1365-246X.2003.02094.x>
- Barklage, M., Wiens, D.A., Nyblade, A. and Anandakrishnan, S. 2009. Upper mantle seismic anisotropy of South Victoria Land and the Ross Sea coast, Antarctica from SKS and SKKS splitting analysis. *Geophysical Journal International*, **178**, 729–741, <https://doi.org/10.1111/j.1365-246X.2009.04158.x>
- Bayer, B., Muller, C., Eaton, D.W. and Jokat, W. 2007. Seismic anisotropy beneath Dronning Maud Land, Antarctica, revealed by shear wave splitting. *Geophysical Journal International*, **171**, 339–351, <https://doi.org/10.1111/j.1365-246X.2007.03519.x>
- Behrendt, J.C. 1999. Crustal and lithospheric structure of the West Antarctic Rift System from geophysical investigations – a review. *Global and Planetary Change*, **23**, 25–44.
- Bentley, C. 1973. Crustal structure of Antarctica. *Tectonophysics*, **20**, 229–240, [https://doi.org/10.1016/0040-1951\(73\)90112-1](https://doi.org/10.1016/0040-1951(73)90112-1)
- Bernacchi, L.C. and Milne, J. 1908. Earthquakes and other earth movements recorded in the Antarctic regions, 1902–1903. In: *National Antarctic Expedition 1901–1904. Physical Observations*. The Royal Society, London, 37–96.
- Bialas, R.W., Buck, W.R., Studinger, M. and Fitzgerald, P.G. 2007. Plateau collapse model for the Transantarctic Mountains–West Antarctic Rift System: insights from numerical experiments. *Geology*, **35**, 687–690, <https://doi.org/10.1130/G23825A.1>
- Bina, C.R. and Helffrich, G. 1994. Phase transition Clapeyron slopes and transition zone seismic discontinuity topography. *Journal of Geophysical Research*, **99**, 15853–15860, <https://doi.org/10.1029/94JB00462>
- Bredow, E. and Steinberger, B. 2021. Mantle convection and possible mantle plumes beneath Antarctica – insights from geodynamic models and implications for topography. *Geological Society, London, Memoirs*, **56**, <https://doi.org/10.1144/M56-2020-2>
- Brenn, G.R., Hansen, S.E. and Park, Y. 2017. Variable thermal loading and flexural uplift along the Transantarctic Mountains, Antarctica. *Geology*, **45**, 463–466, <https://doi.org/10.1130/G38784.1>
- Boger, S.D. 2011. Antarctica – before and after Gondwana. *Precambrian Research*, **19**, 335–371, <https://doi.org/10.1016/j.gr.2010.09.003>
- Bozdač, E., Peter, D. *et al.* 2016. Global adjoint tomography: first-generation model. *Geophysical Journal International*, **207**, 1739–1766, <https://doi.org/10.1093/gji/ggw356>
- Brommer, A., Millar, I.L. and Zeh, A. 1999. Geochronology, structural geology and petrography of the northwestern La Grange Nunataks, Shackleton Range, Antarctica. *Terra Antarctica*, **6**, 269–278.
- Chang, S.-J., Baag, C.-E. and Langston, C.A. 2004. Joint analysis of teleseismic receiver functions and surface wave dispersion using the genetic algorithm. *Bulletin of the Seismological Society of America*, **94**, 691–704, <https://doi.org/10.1785/0120030110>
- Chaput, J., Aoster, R. *et al.* 2014. The crustal thickness of West Antarctica. *Journal of Geophysical Research: Solid Earth*, **119**, 378–395, <https://doi.org/10.1002/2013JB010642>
- Chatzaras, V. and Kruckenberg, S.C. 2021. Effects of melt percolation, refertilization, and deformation on upper mantle seismic anisotropy: constraints from peridotite xenoliths, Marie Byrd Land, West Antarctica. *Geological Society, London, Memoirs*, **56**, <https://doi.org/10.1144/M56-2020-16>
- Chen, M., Huang Yao, H., van der Hilst, R. and Niu, F. 2014. Low wave speed zones in the crust beneath SE Tibet revealed by ambient noise adjoint tomography. *Geophysical Research Letters*, **41**, 334–340, <https://doi.org/10.1002/2013GL058476>
- Cline, C.J., Faul, U.H., David, E.C., Berry, A.J. and Jackson, I. 2018. Redox-influenced seismic properties of upper-mantle olivine. *Nature*, **555**, 355–358, <https://doi.org/10.1038/nature25764>
- Corr, H.F. and Vaughan, D.G. 2008. A recent volcanic eruption beneath the West Antarctic ice sheet. *Nature Geoscience*, **1**, 122–125, <https://doi.org/10.1038/ngeo106>
- Danesi, S. and Morelli, A. 2001. Structure of the upper mantle under the Antarctic Plate from surface wave tomography. *Geophysical Research Letters*, **28**, 4395–4398, <https://doi.org/10.1029/2001GL013431>
- Davey, F.J., Granot, R., Cande, S.C., Stock, J.M., Selvans, M. and Ferraccioli, F. 2016. Synchronous oceanic spreading and continental rifting in West Antarctica. *Geophysical Research Letters*, **43**, 6162–6169, <https://doi.org/10.1002/2016GL069087>
- Day, J.M.D., Harvey, R.P. and Hilton, D.R. 2019. Melt-modified lithosphere beneath Ross Island and its role in the tectono-magmatic evolution of the West Antarctic Rift System. *Chemical Geology*, **518**, 45–54, <https://doi.org/10.1016/j.chemgeo.2019.04.012>
- Eagles, G., Gohl, K. and Larter, R.D. 2004. High-resolution animated tectonic reconstruction of the South Pacific and West Antarctic margin. *Geochemistry, Geophysics, Geosystems*, **5**, Q07004, <https://doi.org/10.1029/2003GC000657>
- Emry, E.L., Nyblade, A.A. *et al.* 2015. The mantle transition zone beneath West Antarctica: seismic evidence for hydration and thermal upwellings. *Geochemistry, Geophysics, Geosystems*, **15**, 40–58, <https://doi.org/10.1002/2014GC005588>
- Emry, E.L., Nyblade, A.A. *et al.* 2020. Prominent thermal anomalies in the mantle transition zone beneath the Transantarctic Mountains. *Geology*, **48**, 748–752, <https://doi.org/10.1130/G47346.1>
- Ferraccioli, F., Finn, C.A., Jordan, T.A., Bell, R.E., Anderson, L.M. and Damaske, D. 2011. East Antarctic rifting triggers uplift of the Gamburtsev Mountains. *Nature*, **479**, 388–392, <https://doi.org/10.1038/nature10566>
- Fielding, C.R., Whittaker, J., Henrys, S.A., Wilson, T.J. and Naish, T.R. 2008. Seismic facies and stratigraphy of the Cenozoic succession in McMurdo Sound, Antarctica: implications for tectonic, climatic and glacial history. *Palaeogeography, Palaeoclimatology, Palaeoecology*, **260**, 8–29, <https://doi.org/10.1016/j.palaeo.2007.08.016>
- Finn, C.A., Müller, R.D. and Panter, K.S. 2005. A Cenozoic diffuse alkaline magmatic province (DAMP) in the southwest Pacific without rift or plume origin. *Geochemistry, Geophysics, Geosystems*, **6**, Q02005, <https://doi.org/10.1029/2004GC000723>
- Fichtner, A., Kennett, B.L., Igel, H. and Bunge, H.P. 2009. Full seismic waveform tomography for upper-mantle structure in the Australasian region using adjoint methods. *Geophysical Journal International*, **179**, 1703–1725, <https://doi.org/10.1111/j.1365-246X.2009.04368.x>
- Fitzsimons, I.C.W. 2000. A review of tectonic events in the East Antarctic shield and their implications for Gondwana and earlier supercontinents. *Journal of African Earth Sciences*, **31**, 3–23, [https://doi.org/10.1016/S0899-5362\(00\)00069-5](https://doi.org/10.1016/S0899-5362(00)00069-5)
- Foley, S.F., Andronikov, A.V., Jacob, D.E. and Melzer, S. 2006. Evidence from Antarctic mantle peridotite xenoliths for changes in mineralogy, geochemistry and geothermal gradients beneath a developing rift. *Geochimica et Cosmochimica Acta*, **70**, 3096–3120, <https://doi.org/10.1016/j.gca.2006.03.010>
- Foley, S.F., Andronikov, A.V., Halpin, J.A., Daczko, N.R. and Jacob, D.E. 2021. Mantle rocks in East Antarctica. *Geological Society, London, Memoirs*, **56**, <https://doi.org/10.1144/M56-2020-8>
- Forsyth, D.W. and Li, A. 2005. Array analysis of two-dimensional variations in surface wave phase velocity and azimuthal anisotropy in the presence of multipathing interference, in seismic earth: array analysis of broadband seismograms. *American Geophysical Union Geophysical Monograph Series*, **157**, 81–97.

Seismic structure of the Antarctic upper mantle

- French, S.W. and Romanowicz, B. 2015. Broad plumes rooted at the base of the Earth's mantle beneath major hotspots. *Nature*, **525**, 95–99, <https://doi.org/10.1038/nature14876>
- Fretwell, P., Pritchard, H.D. *et al.* 2013. Bedmap2: improved ice bed, surface and thickness datasets for Antarctica. *The Cryosphere*, **7**, 375–393, <https://doi.org/10.5194/tc-7-375-2013>
- Gomez, N., Pollard, D. and Holland, D. 2015. Sea-level feedback lowers projections of future Antarctic ice sheet mass loss. *Nature Communications*, **6**, 8798, <https://doi.org/10.1038/ncomms9798>
- Goodge, J.W. and Fanning, C.M. 1999. 2.5 b.y. of punctuated Earth history as recorded in a single rock. *Geology*, **27**, 1007–1010, [https://doi.org/10.1130/0091-7613\(1999\)027<1007:BYOPEH>2.3.CO;2](https://doi.org/10.1130/0091-7613(1999)027<1007:BYOPEH>2.3.CO;2)
- Goodge, J.W. and Fanning, C.M. 2016. Mesoarchean and Paleoproterozoic history of the Nimrod Complex, central Transantarctic Mountains, Antarctica: Stratigraphic revisions and relation to the Mawson Continent in East Gondwana. *Precambrian Research*, **285**, 242–271, <https://doi.org/10.1016/j.precamres.2016.09.001>
- Goodge, J.W., Fanning, C.M. and Bennett, V.C. 2001. U-Pb evidence of c. 1.7 Ga crustal tectonism during the nimrod orogeny in the Transantarctic Mountains, Antarctica: implications for Proterozoic plate reconstructions. *Precambrian Research*, **112**, 261–288, [https://doi.org/10.1016/S0301-9268\(01\)00193-0](https://doi.org/10.1016/S0301-9268(01)00193-0)
- Goodge, J.W., Fanning, C.M., Fisher, C.M. and Vervoort, J.D. 2017. Proterozoic crustal evolution of central East Antarctica: age and isotopic evidence from glacial igneous clasts, and links with Australia and Laurentia. *Precambrian Research*, **299**, 151–176, <https://doi.org/10.1016/j.precamres.2017.07.026>
- Granot, R. and Dyment, J. 2018. Late Cenozoic unification of East and West Antarctica. *Nature Communications*, **9**, 3189, <https://doi.org/10.1038/s41467-018-05270-w>
- Granot, R., Cande, S.C., Stock, J.M. and Damaske, D. 2013. Revised Eocene–Oligocene kinematics for the West Antarctic rift system. *Geophysical Research Letters*, **40**, 279–284, <https://doi.org/10.1029/2012GL054181>
- Graw, J.H., Adams, A.N., Hansen, S.E., Wiens, D.A., Hackworth, L. and Park, Y. 2016. Upper mantle shear wave velocity structure beneath northern Victoria Land, Antarctica: volcanism and uplift in the northern Transantarctic Mountains. *Earth and Planetary Science Letters*, **449**, 48–60, <https://doi.org/10.1016/j.epsl.2016.05.026>
- Groome, W.G. and Thorkelson, D.J. 2009. The three-dimensional thermo-mechanical signature of ridge subduction and slab window migration. *Tectonophysics*, **464**, 70–83, <https://doi.org/10.1016/j.tecto.2008.07.003>
- Grunow, A.M., Kent, D.V. and Dalziel, I.W.D. 1987. Mesozoic evolution of West Antarctica and the Weddell Sea basin: new paleomagnetic constraints. *Earth and Planetary Science Letters*, **86**, 16–26, [https://doi.org/10.1016/0012-821X\(87\)90184-1](https://doi.org/10.1016/0012-821X(87)90184-1)
- Handler, M.R., Wysoczanski, R.J. and Gamble, J.A. 2021. Marie Byrd Land lithospheric mantle: A review of the xenolith record. *Geological Society, London, Memoirs*, **56**, <https://doi.org/10.1144/M56-2020-17>
- Hansen, S.E., Julia, J., Nyblade, A.A., Pyle, M.L., Wiens, D.A. and Anandakrishnan, S. 2009. Using S wave receiver functions to estimate crustal structure beneath ice sheets: An application to the Transantarctic Mountains and East Antarctic craton. *Geochemistry, Geophysics, Geosystems*, **10**, Q08014, <https://doi.org/10.1029/2009GC002576>
- Hansen, S.E., Nyblade, A.A., Heeszel, D.S., Wiens, D.A., Shore, P. and Kanao, M. 2010. Crustal structure of the Gamburtsev Mountains, East Antarctica, from S-wave receiver functions and Rayleigh wave phase velocities. *Earth and Planetary Science Letters*, **300**, 395–401, <https://doi.org/10.1016/j.epsl.2010.10.022>
- Hansen, S.E., Graw, J.H. *et al.* 2014. Imaging the Antarctic mantle using adaptively parameterized P-wave tomography: evidence for heterogeneous structure beneath West Antarctica. *Earth and Planetary Science Letters*, **408**, 66–78, <https://doi.org/10.1016/j.epsl.2014.09.043>
- Hansen, S.E., Reusch, A.M., Parker, T., Bloomquist, D.K., Carpenter, P., Graw, J.H. and Brenn, G.R. 2015. The Transantarctic Mountains Northern Network (TAMNNET): deployment and performance of a seismic array in Antarctica. *Seismological Research Letters*, **86**, 1636–1644, <https://doi.org/10.1785/0220150117>
- Heeszel, D.S., Wiens, D.A., Nyblade, A.A., Hansen, S.E., Kanao, M., An, M. and Zhao, Y. 2013. Rayleigh wave constraints on the structure and tectonic history of the Gamburtsev Subglacial Mountains, East Antarctica. *Journal of Geophysical Research*, **118**, 2138–2153, <https://doi.org/10.1002/jgrb.50171>
- Heeszel, D.S., Wiens, D.A. *et al.* 2016. Upper mantle structure of central and West Antarctica from array analysis of Rayleigh wave phase velocities. *Journal of Geophysical Research: Solid Earth*, **121**, 1758–1775, <https://doi.org/10.1002/2015JB012616>
- Hole, M.J. and LeMasurier, W.E. 1994. Tectonic controls on the geochemical composition of Cenozoic mafic alkaline volcanic rocks from West Antarctica. *Contributions to Mineralogy and Petrology*, **117**, 187–202, <https://doi.org/10.1007/BF00286842>
- Huerta, A.D. 2007. Lithospheric structure across the Transantarctic Mountains constrained by analysis of gravity and thermal structure. *United States Geological Survey Open-File Report*, **2007-1047**, <https://doi.org/10.3133/of2007-1047.srp022>
- Ivins, E.R. and James, T.S. 2005. Antarctic glacial isostatic adjustment: a new assessment. *Antarctic Science*, **17**, 537–549, <https://doi.org/10.1017/S0954102005002968>
- Ivins, E.R. and Sammis, C.G. 1995. On lateral viscosity contrast in the mantle and the rheology of low-frequency geodynamics. *Geophysical Journal International*, **123**, 305–322, <https://doi.org/10.1111/j.1365-246X.1995.tb06856.x>
- Ivins, R.E., van der Wal, W., Wiens, D., Lloyd, A. and Caron, L. In press. Antarctic upper mantle rheology. *Geological Society, London, Memoirs*, **56**, <https://doi.org/10.1144/M56-2020-19>
- Jacobs, J., Bingen, B., Thomas, R.J., Bauer, W., Wingate, M.T.D. and Feitio, P. 2008. Early Palaeozoic orogenic collapse and voluminous late-tectonic magmatism in Dronning Maud Land and Mozambique: insights into the partially delaminated orogenic root of the East African–Antarctic Orogen? *Geological Society, London, Special Publications*, **308**, 69–90, <https://doi.org/10.1144/SP308.3>
- Jordan, T.A., Ferraccioli, F. *et al.* 2013. Inland extent of the Weddell Sea Rift imaged by new aerogeophysical data. *Tectonophysics*, **585**, 137–160, <https://doi.org/10.1016/j.tecto.2012.09.010>
- Jordan, T.A., Ferraccioli, F. and Leat, P.T. 2017. New geophysical compilations link crustal block motion to Jurassic extension and strike-slip faulting in the Weddell Sea Rift System of West Antarctica. *Gondwana Research*, **42**, 29–48, <https://doi.org/10.1016/j.gr.2016.09.009>
- Jordan, T.H. 1981. Continents as a chemical boundary layer. *Philosophical Transactions of the Royal Society A: Mathematical, Physical and Engineering Sciences*, **301**, 359–373, <https://doi.org/10.1098/rsta.1981.0117>
- Julia, J., Ammon, C.J., Herrmann, R.B. and Correig, A.M. 2000. Joint inversion of receiver function and surface wave dispersion observations. *Geophysical Journal International*, **143**, 99–112, <https://doi.org/10.1046/j.1365-246x.2000.00217.x>
- Karato, S., Jung, H., Katayama, I. and Skemer, P. 2008. Geodynamic significance of seismic anisotropy of the upper mantle: new insights from laboratory studies. *Annual Review of Earth and Planetary Sciences*, **36**, 59–95, <https://doi.org/10.1146/annurev.earth.36.031207.124120>
- Komatitsch, D. and Tromp, J. 1999. Introduction to the spectral element method for three-dimensional seismic wave propagation. *Geophysical Journal International*, **139**, 806–822, <https://doi.org/10.1046/j.1365-246x.1999.00967.x>
- Komatitsch, D. and Tromp, J. 2002a. Spectral-element simulations of global seismic wave propagation – I. Validation. *Geophysical Journal International*, **149**, 390–412, <https://doi.org/10.1046/j.1365-246x.2002.01653.x>
- Komatitsch, D. and Tromp, J. 2002b. Spectral-element simulations of global seismic wave propagation – II. Three-dimensional

- models, oceans, rotation and self-gravitation. *Geophysical Journal International*, **150**, 303–318, <https://doi.org/10.1046/j.1365-246X.2002.01716.x>
- Komatitsch, D. and Vilotte, J.P. 1998. The spectral element method: An efficient tool to simulate the seismic response of 2D and 3D geological structures. *Bulletin of the Seismological Society of America*, **88**, 368–392.
- Kustowski, B., Ekström, G. and Dziewoński, A.M. 2008. Anisotropic shear-wave velocity structure of the Earth's mantle: a global model. *Journal of Geophysical Research: Solid Earth*, **113**, <https://doi.org/10.1029/2007JB005169>
- Kyle, P.R. 1990. McMurdo Volcanic Group, western Ross Embayment: introduction. *American Geophysical Union Antarctic Research Series*, **48**, 19–25.
- Kyle, P.R., Moore, J.A. and Thirlwall, M.F. 1992. Petrologic evolution of anorthoclase phonolite lavas at Mount Erebus, Ross Island, Antarctica. *Journal of Petrology*, **33**, 849–875, <https://doi.org/10.1093/petrology/33.4.849>
- Lawrence, J.F. and Wiens, D.A. 2004. Combined receiver function and surface wave phase velocity inversion using a niching genetic algorithm: application to Patagonia. *Bulletin of the Seismological Society of America*, **94**, 977–987, <https://doi.org/10.1785/0120030172>
- Lawrence, J.F., Wiens, D.A., Nyblade, A.A., Anandakrishnan, S., Shore, P.J. and Voigt, D. 2006a. Rayleigh wave phase velocity analysis of the Ross Sea Transantarctic Mountains, and East Antarctica from a temporary seismograph array. *Journal of Geophysical Research: Solid Earth*, **111**, B06302, <https://doi.org/10.1029/2005JB003812>
- Lawrence, J.F., Wiens, D.A., Nyblade, A.A., Anandakrishnan, S., Shore, P.J. and Voigt, D. 2006b. Upper mantle thermal variations beneath the Transantarctic Mountains inferred from teleseismic S-wave attenuation. *Geophysical Research Letters*, **33**, L03303, <https://doi.org/10.1029/2005GL024516>
- Lawrence, J.F., Wiens, D.A., Nyblade, A.A., Anandakrishnan, S., Shore, P.J. and Voigt, D. 2006c. Crust and upper mantle structure of the Transantarctic Mountains and surrounding regions from receiver functions, surface waves, and gravity: implications for uplift models. *Geochemistry, Geophysics, Geosystems*, **7**, Q10011, <https://doi.org/10.1029/2006GC001282>
- Lee, C.-T.A. 2003. Compositional variation of density and seismic velocities in natural peridotites at STP conditions: implications for seismic imaging of compositional heterogeneities in the upper mantle. *Journal of Geophysical Research*, **108**, 2441, <https://doi.org/10.1029/2003JB002413>
- Leitchenkov, G. and Kudryavtzev, G. 1997. Structure and origin of the Earth's Crust in the Weddell Sea Embayment (beneath the Front of the Filchner and Ronne Ice Shelves) from deep seismic sounding data. *Polarforschung*, **67**, 143–154.
- LeMasurier, W.E. and Landis, C.A. 1996. Mantle-plume activity recorded by low-relief erosion surfaces in West Antarctica and New Zealand. *Geological Society of America Bulletin*, **108**, 1450–1466, [https://doi.org/10.1130/0016-7606\(1996\)108<1450:MPARBL>2.3.CO;2](https://doi.org/10.1130/0016-7606(1996)108<1450:MPARBL>2.3.CO;2)
- LeMasurier, W.E. and Rex, D.C. 1989. Evolution of linear volcanic ranges in Marie Byrd Land, West Antarctica. *Journal of Geophysical Research: Solid Earth*, **94**, 7223–7236, <https://doi.org/10.1029/JB094iB06p07223>
- Levander, A., Schmandt, B. *et al.* 2011. Continuing Colorado Plateau uplift by delamination-style convective lithospheric downwelling. *Nature*, **472**, 461–465, <https://doi.org/10.1038/nature10001>
- Licht, K.J., Groth, T., Townsend, J.P., Hennessy, A.J., Hemming, S.R., Flood, T.P. and Studinger, M. 2018. Evidence for extending anomalous Miocene volcanism at the edge of the East Antarctic craton. *Geophysical Research Letters*, **45**, 3009–3016, <https://doi.org/10.1002/2018GL077237>
- Liu, Y., Niu, F., Chen, M. and Yang, W. 2017. 3-D crustal and uppermost mantle structure beneath NE China revealed by ambient noise adjoint tomography. *Earth and Planetary Science Letters*, **461**, 20–29, <https://doi.org/10.1016/j.epsl.2016.12.029>
- Lloyd, A.J. 2018. *Seismic Tomography of Antarctica and the Southern Oceans: Regional and Continental Models from the Upper Mantle to the Transition Zone*. PhD thesis, Washington University in St Louis, St Louis, MO, USA.
- Lloyd, A.J., Nyblade, A.A., Wiens, D.A., Hansen, S.E., Kanao, M., Shore, P.J. and Zhao, D. 2013. Upper mantle seismic structure beneath central East Antarctica from body wave tomography: implications for the origin of the Gamburtsev Subglacial Mountains. *Geochemistry, Geophysics, Geosystems*, **14**, 902–920, <https://doi.org/10.1002/ggpe.20098>
- Lloyd, A.J., Wiens, D.A. *et al.* 2015. A seismic transect across West Antarctica: Evidence for mantle thermal anomalies beneath the Bentley Subglacial Trench and the Marie Byrd Land Dome. *Journal of Geophysical Research: Solid Earth*, **120**, 8439–8460, <https://doi.org/10.1002/2015JB012455>
- Lloyd, A.J., Wiens, D.A. *et al.* 2020. Seismic structure of the Antarctic upper mantle imaged with adjoint tomography. *Journal of Geophysical Research: Solid Earth*, **125**, <https://doi.org/10.1029/2019JB017823>
- Lough, A.C., Wiens, D.A. *et al.* 2013. Seismic detection of an active subglacial magmatic complex in Marie Byrd Land, Antarctica. *Nature Geoscience*, **6**, 1031–1035, <https://doi.org/10.1038/ngeo1992>
- Lucas, E.M., Nyblade, A. *et al.* 2020a. Upper mantle seismic anisotropy of Antarctica from shear wave splitting analysis. *AGU Fall Meeting Abstracts*, **2020**, T008-03, <https://ui.adsabs.harvard.edu/#abs/2020AGUFMT008...03L/abstract>
- Lucas, E.M., Soto, D. *et al.* 2020b. P- and S-wave velocity structure of central West Antarctica: implications for the tectonic evolution of the West Antarctic Rift System. *Earth and Planetary Science Letters*, **546**, 116437, <https://doi.org/10.1016/j.epsl.2020.116437>
- Mainprice, D. and Silver, P.G. 1993. Interpretation of SKS-waves using samples from the subcontinental lithosphere. *Physics of the Earth and Planetary Interiors*, **78**, 257–280, [https://doi.org/10.1016/0031-9201\(93\)90160-B](https://doi.org/10.1016/0031-9201(93)90160-B)
- Maritati, A., Danišák, M., Halpin, J.A., Whittaker, J.M. and Aitken, A.R.A. 2020. Pangea rifting shaped the East Antarctic landscape. *Tectonics*, **39**, e2020TC006180, <https://doi.org/10.1029/2020TC006180>
- Martin, A.P. and Cooper, A.F. 2010. Post 3.9 Ma fault activity within the West Antarctic rift system: onshore evidence from Gandalf Ridge, Mount Morning eruptive centre, southern Victoria Land, Antarctica. *Antarctic Science*, **22**, 513–521, <https://doi.org/10.1017/S095410201000026X>
- Martin, A.P., Cooper, A.F., Price, R.C., Doherty, C.L. and Gamble, J.A. 2021a. A review of mantle xenoliths in volcanic rocks from southern Victoria Land, Antarctica. *Geological Society, London, Memoirs*, **56**, <https://doi.org/10.1144/M56-2019-42>
- Martin, A.P., Cooper, A.F., Price, R.C., Kyle, P.R. and Gamble, J.A., Smellie, J.L. 2021b. Erebus Volcanic Province: petrology. *Geological Society, London, Memoirs*, **55**, 447–489, <https://doi.org/10.1144/M55-2018-80>
- Muller, C. 2001. Upper mantle seismic anisotropy beneath Antarctica and the Scotia Sea region. *Geophysical Journal International*, **147**, 105–122, <https://doi.org/10.1046/j.1365-246X.2001.00517.x>
- O'Donnell, J.P., Selway, K. *et al.* 2017. The uppermost mantle seismic velocity and viscosity structure of central West Antarctica. *Earth and Planetary Science Letters*, **472**, 38–49, <https://doi.org/10.1016/j.epsl.2017.05.016>
- O'Donnell, J.P., Brisbourne, A.M. *et al.* 2019a. Mapping crustal shear wave velocity structure and radial anisotropy beneath West Antarctica using seismic ambient noise. *Geochemistry, Geophysics, Geosystems*, **20**, 5014–5037, <https://doi.org/10.1029/2019GC008459>
- O'Donnell, J.P., Stuart, G.W. *et al.* 2019b. The uppermost mantle seismic velocity structure of West Antarctica from Rayleigh wave tomography: insights into tectonic structure and geothermal heat flow. *Earth and Planetary Science Letters*, **522**, 219–233, <https://doi.org/10.1016/j.epsl.2019.06.024>

Seismic structure of the Antarctic upper mantle

- Oliver, R.L. and Fanning, C.M. 2002. Proterozoic geology east and southeast of Commonwealth Bay, George V Land, Antarctica, and its relationship to that of adjacent Gondwana terranes. *Royal Society of New Zealand Bulletin*, **35**, 51–58.
- Panning, M. and Romanowicz, B. 2006. A three-dimensional radially anisotropic model of shear velocity in the mantle. *Geophysical Journal International*, **167**, 361–379, <https://doi.org/10.1111/j.1365-246X.2006.03100.x>
- Panter, K.S., Hart, S.R., Kyle, P., Blusztajn, J. and Wilch, T. 2000. Geochemistry of Late Cenozoic basalts from the Crary Mountains: characterization of mantle sources in Marie Byrd Land, Antarctica. *Chemical Geology*, **165**, 215–241, [https://doi.org/10.1016/S0009-2541\(99\)00171-0](https://doi.org/10.1016/S0009-2541(99)00171-0)
- Pappa, F. and Ebbing, J. 2021. Gravity, magnetics and geothermal heat flow of the Antarctic lithospheric crust and mantle. *Geological Society, London, Memoirs*, **56**, <https://doi.org/10.1144/M56-2020-5>
- Pappa, F., Ebbing, J. and Ferraccioli, F. 2019a. Moho depths of Antarctica: comparison of seismic, gravity, and isostatic results. *Geochemistry, Geophysics, Geosystems*, **20**, 1629–1645, <https://doi.org/10.1029/2018GC008111>
- Pappa, F., Ebbing, J., Ferraccioli, F. and van der Wal, W. 2019b. Modeling satellite gravity gradient data to derive density, temperature, and viscosity structure of the antarctic lithosphere. *Journal of Geophysical Research: Solid Earth*, **124**, 12 053–12 076, <https://doi.org/10.1029/2019JB017997>
- Pattyn, F. 2010. Antarctic subglacial conditions inferred from a hybrid ice sheet/ice stream model. *Earth and Planetary Science Letters*, **295**, 451–461, <https://doi.org/10.1016/j.epsl.2010.04.025>
- Paulsen, T.S. and Wilson, T.J. 2010. Evolution of Neogene volcanism and stress patterns in the glaciated West Antarctic Rift, Marie Byrd Land, Antarctica. *Journal of the Geological Society, London*, **167**, 401–416, <https://doi.org/10.1144/0016-76492009-044>
- Paxman, G.J.G. 2021. Antarctic palaeotopography. *Geological Society, London, Memoirs*, **56**, <https://doi.org/10.1144/M56-2020-7>
- Phillips, E.H., Sims, K.W. et al. 2018. The nature and evolution of mantle upwelling at Ross Island, Antarctica, with implications for the source of HIMU lavas. *Earth and Planetary Science Letters*, **498**, 38–53, <https://doi.org/10.1016/j.epsl.2018.05.049>
- Phillips, G. and Laufer, A.L. 2009. Brittle deformation relating to the Carboniferous–Cretaceous evolution of the Lambert Graben, East Antarctica: a precursor for Cenozoic relief development in an intraplate and glaciated region. *Tectonophysics*, **471**, 216–224, <https://doi.org/10.1016/j.tecto.2009.02.012>
- Pollard, D., DeConto, R.M. and Nyblade, A.A. 2005. Sensitivity of Cenozoic Antarctic ice sheet variations to geothermal heat flux. *Global and Planetary Change*, **49**, 63–74, <https://doi.org/10.1016/j.gloplacha.2005.05.003>
- Priestley, K. and McKenzie, D. 2006. The thermal structure of the lithosphere from shear wave velocities. *Earth and Planetary Science Letters*, **244**, 285–301, <https://doi.org/10.1016/j.epsl.2006.01.008>
- Pyle, M.L., Wiens, D.A., Nyblade, A.A. and Anandakrishnan, S. 2010. Crustal structure of the Transantarctic Mountains near the Ross Sea from ambient seismic noise tomography. *Journal of Geophysical Research: Solid Earth*, **115**, B11310, <https://doi.org/10.1029/2009JB007081>
- Ramirez, C., Nyblade, A. et al. 2016. Crustal and upper-mantle structure beneath ice-covered regions in Antarctica from S-wave receiver functions and implications for heat flow. *Geophysical Journal International*, **204**, 1636–1648, <https://doi.org/10.1093/gji/ggv542>
- Ramirez, C., Nyblade, A. et al. 2017. Crustal structure of the Transantarctic Mountains, Ellsworth Mountains and Marie Byrd Land, Antarctica: constraints on shear wave velocities, Poisson's ratios and Moho depths. *Geophysical Journal International*, **211**, 1328–1340, <https://doi.org/10.1093/gji/ggx333>
- Reading, A.M. 2006. The seismic structure of Precambrian and early Palaeozoic terranes in the Lambert Glacier region, East Antarctica. *Earth and Planetary Science Letters*, **244**, 44–57, <https://doi.org/10.1016/j.epsl.2006.01.031>
- Reading, A.M. and Heintz, M. 2008. Seismic anisotropy of East Antarctica from shear-wave splitting: spatially varying contributions from lithospheric structural fabric and mantle flow? *Earth and Planetary Science Letters*, **268**, 433–443, <https://doi.org/10.1016/j.epsl.2008.01.041>
- Reusch, A.M., Nyblade, A.A., Benoit, M.H., Wiens, D.A., Anandakrishnan, S., Voigt, D. and Shore, P.J. 2008. Mantle transition zone thickness beneath Ross Island, the Transantarctic Mountains, and East Antarctica. *Geophysical Research Letters*, **35**, <https://doi.org/10.1029/2008GL033873>
- Ritzwoller, M.H., Shapiro, N.M., Levshin, A.L. and Leahy, G.M. 2001. Crustal and upper mantle structure beneath Antarctica and surrounding oceans. *Journal of Geophysical Research: Solid Earth*, **106**, 30 645–30 670, <https://doi.org/10.1029/2001JB000179>
- Robertson Maurice, S.D., Wiens, D.A., Shore, P.J., Vera, E. and Dorman, L.M. 2003. Seismicity and tectonics of the South Shetland Islands and Bransfield Strait from a regional broadband seismograph deployment. *Journal of Geophysical Research: Solid Earth*, **108**, 2461, <https://doi.org/10.1029/2003JB002416>
- Roult, G., Rouland, D. and Montagner, J.P. 1994. Antarctica II: Upper mantle structure from velocities and anisotropy. *Physics of the Earth and Planetary Interiors*, **84**, 33–57, [https://doi.org/10.1016/0031-9201\(94\)90033-7](https://doi.org/10.1016/0031-9201(94)90033-7)
- Savage, M.K. 1999. Seismic anisotropy and mantle deformation: what have we learned from shear wave splitting? *Reviews of Geophysics*, **37**, 65–106, <https://doi.org/10.1029/98RG02075>
- Schutt, D.L. and Lesher, C.E. 2006. Effects of melt depletion on the density and seismic velocity of garnet and spinel lherzolite. *Journal of Geophysical Research: Solid Earth*, **111**, B05401, <https://doi.org/10.1029/2003JB002950>
- Shapiro, N.M. and Ritzwoller, M.H. 2004. Inferring surface heat flux distributions guided by a global seismic model: Particular application to Antarctica. *Earth and Planetary Science Letters*, **223**, 213–224, <https://doi.org/10.1016/j.epsl.2004.04.011>
- Shapiro, N.M., Campillo, M., Stehly, L. and Ritzwoller, M.H. 2005. High-resolution surface wave tomography from ambient seismic noise. *Science*, **307**, 1615–1618, <https://doi.org/10.1126/science.1108339>
- Shen, W., Wiens, D.A. et al. 2018a. Seismic evidence for lithospheric foundering beneath the southern Transantarctic Mountains, Antarctica. *Geology*, **46**, 71–74, <https://doi.org/10.1130/G39555.1>
- Shen, W., Wiens, D.A. et al. 2018b. The crust and upper mantle structure of central and West Antarctica from Bayesian inversion of Rayleigh wave and receiver functions. *Journal of Geophysical Research: Solid Earth*, **123**, 7824–7849, <https://doi.org/10.1029/2017JB015346>
- Shen, W., Wiens, D.A., Lloyd, A. and Nyblade, A.A. 2020. A geothermal heat flux map of Antarctica empirically constrained by seismic structure. *Geophysical Research Letters*, **47**, e2020GL086955, <https://doi.org/10.1029/2020GL086955>
- Siddoway, C.S. 2008. Tectonics of the West Antarctic Rift System: new light on the history and dynamics of distributed intracontinental extension. In: Cooper, A., Barrett, P.J. et al. (eds) *Antarctica: A Keystone in a Changing World*. National Academy of Sciences, Washington, DC, 91–114.
- Sieminski, A., Debayle, E. and Lévéque, J.J. 2003. Seismic evidence for deep low-velocity anomalies in the transition zone beneath West Antarctica. *Earth and Planetary Science Letters*, **216**, 645–661, [https://doi.org/10.1016/s0012-821x\(03\)00518-1](https://doi.org/10.1016/s0012-821x(03)00518-1)
- Silver, P.G. 1996. Seismic anisotropy beneath the continents: probing the depths of geology. *Annual Review of Earth and Planetary Sciences*, **24**, 385–432, <https://doi.org/10.1146/annurev.earth.24.1.385>
- Sleep, N.H. 2005. Evolution of continental lithosphere. *Annual Review of Earth and Planetary Sciences*, **33**, 369–393, <https://doi.org/10.1146/annurev.earth.33.092203.122643>
- Stump, E., Sheridan, M.F., Borg, S.G. and Sutter, J.F. 1980. Early Miocene subglacial basalts, the East Antarctic ice sheet, and

- uplift of the Transantarctic Mountains. *Science*, **207**, 757–759, <https://doi.org/10.1126/science.207.4432.757>
- Sutherland, R., Spasojevic, S. and Gurnis, M. 2010. Mantle upwelling after Gondwana subduction death explains anomalous topography and subsidence histories of eastern New Zealand and West Antarctica. *Geology*, **38**, 155–158, <https://doi.org/10.1130/G30613.1>
- Swain, G., Woodhouse, A., Hand, M., Barovich, K., Schwarz, M. and Fanning, C.M. 2005. Provenance and tectonic development of the late Archaean Gawler Craton, Australia; U-Pb zircon, geochemical and Sm–Nd isotopic implications. *Precambrian Research*, **141**, 106–136, <https://doi.org/10.1016/j.precamres.2005.08.004>
- Szwillus, W., Afonso, J.C.C., Ebbing, J. and Mooney, W.D. 2019. Global crustal thickness and velocity structure from geostatistical analysis of seismic data. *Journal of Geophysical Research: Solid Earth*, **124**, 1626–1652, <https://doi.org/10.1029/2018JB016593>
- Tape, C., Liu, Q., Maggi, A. and Tromp, J. 2010. Seismic tomography of the southern California crust based on spectral-element and adjoint methods. *Geophysical Journal International*, **180**, 433–462, <https://doi.org/10.1111/j.1365-246X.2009.04429.x>
- Tarantola, A. 1984. Inversion of seismic reflection data in the acoustic approximation. *Geophysics*, **49**, 1259–1266, <https://doi.org/10.1190/1.1441754>
- ten Brink, U.S., Bannister, S., Beaudoin, B.C. and Stern, T.A. 1993. Geophysical investigations of the tectonic boundary between East and West Antarctica. *Science*, **261**, 45–50, <https://doi.org/10.1126/science.261.5117.45>
- ten Brink, U.S., Hackney, R.I., Bannister, S., Stern, T.A. and Makovsky, Y. 1997. Uplift of the Transantarctic Mountains and the bedrock beneath the East Antarctic ice sheet. *Journal of Geophysical Research: Solid Earth*, **102**, 27 603–27 621, <https://doi.org/10.1029/97JB02483>
- Tingey, R.J. 1991. The regional geology of Archean and Proterozoic rocks in Antarctica. In: Tingey, R.J. (ed.) *The Geology of Antarctica*. Clarendon Press, Oxford, UK, 1–73.
- Tinto, K.J., Padman, L. *et al.* 2019. Ross Ice Shelf response to climate driven by the tectonic imprint on seafloor bathymetry. *Nature Geoscience*, **12**, 441–449, <https://doi.org/10.1038/s41561-019-0370-2>
- Trey, H., Cooper, A., Pellis, G., della Vedova, B., Cochrane, G., Brancolini, G. and Makris, J. 1999. Transect across the West Antarctic rift system in the Ross Sea, Antarctica. *Tectonophysics*, **301**, 61–74, [https://doi.org/10.1016/S0040-1951\(98\)00155-3](https://doi.org/10.1016/S0040-1951(98)00155-3)
- Tromp, J., Tape, C. and Liu, Q. 2005. Seismic tomography, adjoint methods, time reversal and banana–doughnut kernels. *Geophysical Journal International*, **160**, 195–216, <https://doi.org/10.1111/j.1365-246X.2004.02453.x>
- van de Flierdt, T., Hemming, S.R., Goldstein, S.L., Gehrels, G.E. and Cox, S.E. 2008. Evidence against a young volcanic origin of the Gamburtsev Subglacial Mountains, Antarctica. *Geophysical Research Letters*, **35**, L21303, <https://doi.org/10.1029/2008GL035564>
- van der Lee, S. 2002. High-resolution estimates of lithospheric thickness from Missouri to Massachusetts, USA. *Earth and Planetary Science Letters*, **203**, 15–23, [https://doi.org/10.1016/S0012-821X\(02\)00846-4](https://doi.org/10.1016/S0012-821X(02)00846-4)
- van der Wal, W., Whitehouse, P.L. and Schrama, E.J.O. 2015. Effect of GIA models with 3D composite mantle viscosity on GRACE mass balance estimates for Antarctica. *Earth and Planetary Science Letters*, **414**, 134–143, <https://doi.org/10.1016/j.epsl.2015.01.001>
- Wannamaker, P., Hill, G. *et al.* 2017. Uplift of the central transantarctic mountains. *Nature Communications*, **8**, 1588, <https://doi.org/10.1038/s41467-017-01577-2>
- Watson, T., Nyblade, A. *et al.* 2006. P and S velocity structure of the upper mantle beneath the Transantarctic Mountains, East Antarctic craton, and Ross Sea from travel time tomography. *Geochemistry, Geophysics, Geosystems*, **7**, Q07005, <https://doi.org/10.1029/2005GC001238>
- Weaver, S.D., Storey, B.C., Pankhurst, R.J., Mukasa, S.B., DiVenere, V.J. and Bradshaw, J.D. 1994. Antarctica–New Zealand rifting and Marie Byrd Land lithospheric magmatism linked to ridge subduction and mantle plume activity. *Geology*, **22**, 811–814, [https://doi.org/10.1130/0091-7613\(1994\)022<0811:ANZRAM>2.3.CO;2](https://doi.org/10.1130/0091-7613(1994)022<0811:ANZRAM>2.3.CO;2)
- White-Gaynor, A.L., Nyblade, A.A. *et al.* 2019. Heterogeneous upper mantle structure beneath the Ross Sea Embayment and Marie Byrd Land, West Antarctica, revealed by P-wave tomography. *Earth and Planetary Science Letters*, **513**, 40–50, <https://doi.org/10.1016/j.epsl.2019.02.013>
- Whitehouse, P.L., Gomez, N., King, M.A. and Wiens, D.A. 2019. Solid Earth change and the evolution of the Antarctic Ice Sheet. *Nature Communications*, **10**, 503, <https://doi.org/10.1038/s41467-018-08068-y>
- Wilch, T.I., McIntosh, W.C. and Dunbar, N.W. 1999. Late Quaternary volcanic activity in Marie Byrd Land: potential $^{40}\text{Ar}/^{39}\text{Ar}$ -dated time horizons in West Antarctic ice and marine cores. *Geological Society of America Bulletin*, **111**, 1563–1580, [https://doi.org/10.1130/0016-7606\(1999\)111<1563:LQVAIM>2.3.CO;2](https://doi.org/10.1130/0016-7606(1999)111<1563:LQVAIM>2.3.CO;2)
- Will, T.M., Zeh, A., Gerdes, A., Frimmel, H.E., Millar, I.L. and Schmädicke, E. 2009. Palaeoproterozoic to Palaeozoic magmatic and metamorphic events in the Shackleton Range, East Antarctica: constraints from zircon and monazite dating, and implications for the amalgamation of Gondwana. *Precambrian Research*, **182**, 25–45, <https://doi.org/10.1016/j.precamres.2009.03.008>
- Wilson, D.S. and Luyendyk, B.P. 2009. West Antarctic paleotopography estimated at the Eocene-Oligocene climate transition. *Geophysical Research Letters*, **36**, L16302, <https://doi.org/10.1029/2009GL039297>
- Wobbe, F., Gohl, K., Chambord, A. and Sutherland, R. 2012. Structure and breakup history of the rifted margin of West Antarctica in relation to Cretaceous separation from Zealandia and Bellingshausen plate motion. *Geochemistry, Geophysics, Geosystems*, **13**, Q04W12, <https://doi.org/10.1029/2011GC003742>
- Wobbe, F., Lindeque, A. and Gohl, K. 2014. Anomalous South Pacific lithosphere dynamics derived from new total sediment thickness estimates off the West Antarctic margin. *Global and Planetary Change*, **123**, 139–149, <https://doi.org/10.1016/j.gloplacha.2014.09.006>
- Yamasaki, T., Miura, H. and Nogi, Y. 2008. Numerical modelling study on the flexural uplift of the Transantarctic Mountains. *Geophysical Journal International*, **174**, 377–390, <https://doi.org/10.1111/j.1365-246X.2008.03815.x>
- Yuan, Y.O., Simons, F.J. and Tromp, J. 2016. Double-difference adjoint seismic tomography. *Geophysical Journal International*, **206**, 1599–1618, <https://doi.org/10.1093/gji/ggw233>
- Zhang, S. and Karato, S. 1995. Lattice preferred orientation of olivine aggregates deformed in simple shear. *Nature*, **375**, 774–777, <https://doi.org/10.1038/375774a0>
- Zhou, Z., Wiens, D.A., Shen, W., Hansen, S., Aster, R. and Nyblade, A. 2019. Radial anisotropy of Antarctica from surface wave ambient noise tomography. *Seismological Research Letter*, **90**, 1047.
- Zhu, H., Bozdağ, E. and Tromp, J. 2015. Seismic structure of the European upper mantle based on adjoint tomography. *Geophysical Journal International*, **201**, 18–52, <https://doi.org/10.1093/gji/ggu492>